Structural Vibration Control Using Extension and Shear Active-Passive Piezoelectric Networks Including Sensitivity to Electrical Uncertainties

Heinsten F. L. dos Santos

hfleal@sc.usp.br
Department of Mechanical Engineering
São Carlos School of Engineering
University of São Paulo
13566-590 São Carlos, SP, Brazil

Marcelo A. Trindade

trindade@sc.usp.br
Department of Mechanical Engineering
São Carlos School of Engineering
University of São Paulo
13566-590 São Carlos, SP, Brazil

Active-Passive Piezoelectric Networks (APPN) integrate active voltage sources with passive resistance-inductance shunt circuits to a piezoelectric patch. This technique allows to simultaneously passively dissipate vibratory energy through the shunt circuit and actively control the structural vibrations. This work presents an analysis of active-passive damping performance of beams with extension and shear APPN. A coupled finite element model with mechanical and electrical degrees of freedom is developed and used to design passive and active control parameters. Then, stochastic modeling and analyses of two cantilever beam configurations, with extension and shear APPN, are performed to evaluate the effect of uncertainties in circuit components on passive and active-passive vibration control. Results show that active-passive shunt circuits can be very interesting since they may combine an adequate passive control performance with an increase of active control authority when a control voltage is applied to the circuit. For the extension configuration, vibration amplitude reductions of up to 22 dB and 28 dB are obtained for passive and active-passive cases, respectively. Considering relative dispersions of 10% for the resistance and inductance values, the passive and active-passive amplitude reductions are found to be in the ranges 16-24 dB and 27-28 dB, respectively. For the shear configuration, increases in the active control authority of up to 29 dB due to a properly tuned resonant circuit are observed. When subjected to uncertainties in the resistance and inductance values, with 10% relative dispersions, the control authority increase is in the range of 6-29 dB.
Keywords: *piezoelectric materials, active-passive piezoelectric networks, vibration control, stochastic modeling, uncertainty analysis*

Introduction

Due to their strong electromechanical coupling, piezoelectric materials have been widely used as sensors and actuators for structural vibration control. They can be used either as actuators connected to an appropriate control law to provide active vibration control or as sensors connected to shunt circuits to provide passive damping. In the last decade, research was redirected to combined active and passive vibration control techniques. One of these techniques, so-called Active-Passive Piezoelectric Networks (APPN), integrates an active voltage source with a passive resistance-inductance shunt circuit to a piezoelectric sensor/actuator (Tsai and Wang, 1999). In this case, the piezoelectric material serves two purposes. First, the vibration strain energy of the structure can be transferred to the shunt circuit, through the difference of electric potential induced in the piezoelectric material electrodes, and then passively dissipated in the electric components of the shunt circuit (Forward, 1979; Hagood and von Flotow, 1991, Viana and Steffen, 2006). On the other hand, the piezoelectric material may also serve as an actuator for which a control voltage can be applied to actively control the structural vibrations. This active mechanism combined to a velocity feedback, for instance, may then induce an additional active damping in the structure.

There are still some unresolved issues concerning this active-passive damping mechanism, such as for which conditions simultaneous active-passive damping outperforms separate active and passive mechanisms, that is, whether the control voltage should be part of the shunt circuit or not (Thornburgh and Chattopadhyay, 2003). It has been shown that combined active-passive vibration control allows better performance with smaller cost than separate active and passive control, provided the simultaneous action is optimized (Tsai and Wang, 1999). On the other hand, like for purely passive shunted piezoelectric damping, most of the studies concerning APPN focus on the optimization of the electric circuit architecture and components. It is well-known, however, that the performance of both active and passive damping mechanisms is highly dependent on the effective electromechanical coupling provided by the piezoelectric actuators/sensors. Nevertheless, few studies focus on the optimization of this coupling for given structure and piezoelectric material. In particular, it has been shown that piezoelectric actuators using their thickness-shear mode can be more effective than surface-mounted extension piezoelectric actuators for both active (Trindade, Benjeddou and Ohayon, 1999; Raja, Prathap and Sinha, 2002; Baillargeon and Vel, 2005; Trindade and Benjeddou, 2006) and passive (Benjeddou and Ranger-Vieillard, 2004; Benjeddou, 2007; Trindade and Maio, 2008) vibration damping. One of the reasons for that is the thickness-shear electromechanical coupling coefficient k_{15} that is normally twice the value of the extension one, k_{31}, which may lead to a higher effective electromechanical coupling coefficient (Trindade and Benjeddou, 2009). The thickness-shear mode, originally proposed by Sun and Zhang (1995), can be obtained using longitudinally-poled piezoelectric patches that couple through-thickness electric fields/displacements and shear strains/stresses. On the other hand, although it is well-known that the performance of shunt circuits is quite sensible to the tuning of circuit parameters, little has been published about the complexities in tuning the electric circuit parameters and the effect of the parametric variations on the overall performance of the system (Viana and Steffen, 2006; Andreaus and Porfiri, 2007).

This work presents the modeling of sandwich structures with APPN using extension and thickness-shear piezoelectric sensors/actuators. The model is based on a stress-voltage electromechanical model for the piezoelectric materials fully coupled with the APPN active-passive circuit. To this end, the APPN

Paper received 5 August 2010. Paper accepted 5 February 2011.
Technical Editor: Francisco Cunha

circuit equations are also included in the variational formulation. Hence, conservation of charge and full electromechanical coupling are guaranteed. The formulation results in a coupled finite element model with mechanical (displacements) and electrical (electrodes charges) degrees of freedom. An analysis of the resulting coupled equations of motion is performed to identify the damping mechanisms provided by an active-passive piezoelectric network. Then, stochastic modeling and analysis of two cantilever beam configurations, with extension and shear piezoceramics, are performed to account for uncertainties in circuit components. This work includes an original modeling and analysis of APPN using shear response mode of piezoelectric materials and also an original sensitivity analysis of passive and active-passive shunted piezoelectric damping using a stochastic model.

Nomenclature

A = *cross-sections or electrodes area*
$\mathbf{b}$ = *perturbation input distribution vector*
$\mathbf{C}$ = *damping matrix*
$\mathbf{c}$ = *output distribution vector*
$\bar{c}_{11}^{Dk}$ = *effective elastic stiffness constant of surface layer k*
$\bar{c}_{33}^{Dc}$ = *effective elastic stiffness constant of core layer*
$\mathbf{D}$ = *vector of electric displacements dof*
D_3 = *transverse electric displacement*
E_3 = *transverse electric field*
$\mathbf{F}$ = *vector of generalized mechanical forces*
f = *amplitude of perturbation input*
G_c = *control authority of pair patch and shunt circuit*
G_h = *FRF for beams with active-passive shunt circuits*
G_p = *FRF for beams with passive shunt circuits*
$\mathbf{g}$ = *vector of control gains*
H = *electric enthalpy*
$\bar{h}_{31}^{k}$ = *effective piezoelectric constant of surface layer k*
h_{15}^{c} = *effective piezoelectric constant of core layer*
h = *thickness*
I = *second moment of cross-section area*
$\mathbf{K}$ = *stiffness matrix*
$\bar{\mathbf{K}}$ = *modified stiffness matrix*
k_e = *effective stiffness coefficient of pair patch-circuit*
k_p = *effective piezoelectric stiffness of vibration mode of interest*
L = *length of the beam*
L_{cj} = *inductance of circuit j*
$\mathbf{M}$ = *mass matrix*
m_q = *effective inertia coefficient of pair patch-circuit*
p_X = *probability density function of random variable X*
$\mathbf{q}_c$ = *vector of electric charges generated at piezo-patches*
R_{cj} = *resistance of circuit j*
$\mathbf{u}$ = *vector of nodal mechanical displacements*
u = *axial displacement*
T = *kinetic energy*
V_{cj} = *voltage source applied to circuit j*
W = *work done by dissipative forces*
w = *transverse displacement*
y = *mechanical response output*

Greek Symbols

α_n = *modal displacement of vibration mode of interest*
$\bar{\beta}_{33}^{\varepsilon k}$ = *effective dielectric constant of surface layer k*
$\beta_{11}^{\varepsilon c}$ = *effective dielectric constant of core layer*
β_i = *cross-section rotation angle*
δ = *virtual variation operator*
δ_X = *relative dispersion of random variable X*
ε_1 = *normal strain*
ε_5 = *shear strain*
$\boldsymbol{\phi}_n$ = *vibration mode of interest*
ω = *resonance frequency*
ρ_i = *mass density of layer i*
σ_1 = *normal stress*
σ_5 = *shear stress*
σ_X = *standard deviation of random variable X*

Subscripts

c = *relative to electric shunt circuits*
e = *relative to dielectric contributions or electric circuit*
i = *relative to layer i*
j = *relative to circuit j*
L = *relative to shunt circuit inductance*
m = *relative to mechanical contributions*
me = *relative to piezoelectric contributions*
n = *relative to vibration mode n*
p = *relative to piezoelectric patch p*
q = *relative to electric displacement dofs*
R = *relative to shunt circuit resistance*

Superscripts

c = *relative to core layer or shear strain*
D = *for constant electric displacement*
ε = *for constant strain*
f = *relative to bending strain*
k = *relative to surface layer k*
m = *relative to membrane strain*
OC = *relative to open-circuited shunt circuit*
R = *relative to resistive shunt circuit*
RL = *relative to resonant shunt circuit*
SC = *relative to short-circuited shunt circuit*
V = *relative to voltage source only*

Finite Element Model of a Piezoelectric Sandwich Beam

Consider a sandwich beam made of piezoelectric layers and modeled using a classical sandwich theory. Surface layers are made of transversely poled piezoelectric materials, whereas the core layer is made of longitudinally poled piezoelectric materials. Electrodes fully cover the top and bottom skins of all layers so that only through-thickness electric field and displacement are considered. For simplicity, all layers are assumed to be made of orthotropic piezoelectric materials, perfectly bonded and in plane stress state. Bernoulli-Euler theory is retained for the sandwich beam surface layers, while the core is assumed to behave as a Timoshenko beam. The length, width and thickness of the beam are denoted by L, b and h, respectively.

Displacements and strains

The axial and transverse displacement fields of faces and core may be written in the following general form:

$$\begin{aligned}&\bar{u}_i(x,y,z) = u_i(x) + (z-z_i)\beta_i(x)\ , \quad i = t,c,b,\\ &\bar{v}_i(x,y,z) = 0,\\ &\bar{w}_i(x,y,z) = w(x),\end{aligned} \tag{1}$$

where u_i is the mid-plane axial displacement of the layer i ($i = t$ for the top layer, $i = c$ for the core layer and $i = b$ for the bottom layer). β_i is the cross-section rotation angle and from Bernoulli-Euler assumptions $\beta_t = \beta_b = -w'$, where w' states for $\partial w/\partial x$. z_i states for the position of the layer i mid-plane in the global transversal z direction. Using the displacement continuity conditions between layers, the displacement fields may be written in terms of only three main variables, u_t, u_b and w, so that u_c and β_c are written as

$$u_c = \frac{u_t+u_b}{2} + \frac{h_d}{4}w' \quad \text{and} \quad \beta_c = \frac{u_t-u_b}{h_c} + \frac{h_m}{h_c}w', \tag{2}$$

with h_m and h_d being the mean and difference of the surface layers thicknesses, h_t and h_b:

$$h_m = \frac{h_t+h_b}{2} \quad \text{and} \quad h_d = h_t - h_b. \tag{3}$$

The usual strain-displacement relations for each layer yield the following axial and shear strains for the layer i:

$$\varepsilon_{1i} = \frac{\partial \bar{u}_i}{\partial x} = \varepsilon_i^m + (z-z_i)\varepsilon_i^f \quad \text{and} \quad \varepsilon_{5i} = \frac{\partial \bar{u}_i}{\partial z} + \frac{\partial \bar{w}_i}{\partial x} = \varepsilon_i^c, \tag{4}$$

while the remaining strains ε_{2i}, ε_{3i}, ε_{4i} and ε_{6i} vanish. The membrane, bending and shear generalized strains, ε_i^m, ε_i^f and ε_i^c, can be written as

$$\varepsilon_k^m = u_k',\ \varepsilon_k^f = -w'',\ \varepsilon_k^c = 0, \ \text{ for surface layers } (k = t,b), \tag{5}$$

$$\begin{aligned}&\varepsilon_c^m = \frac{u_t'+u_b'}{2} + \frac{h_d}{4}w'',\ \varepsilon_c^f = \frac{u_t'-u_b'}{h_c} + \frac{h_m}{h_c}w'',\\ &\varepsilon_c^c = \frac{u_t-u_b}{h_c} + \left(\frac{h_m}{h_c}+1\right)w'.\end{aligned} \tag{6}$$

Alternatively, these expressions can be written in terms of the mean and relative axial displacements, instead of the axial displacements of the top and bottom layers, as done in previous works (Benjeddou, Trindade and Ohayon, 1999; Trindade, Benjeddou and Ohayon, 2001).

Piezoelectric constitutive equations

Linear orthotropic piezoelectric materials with material symmetry axes parallel to the beam ones are considered here. The constitutive equations for these materials can be obtained starting from the general expression for the electric enthalpy of a piezoelectric layer

$$H(\boldsymbol{\varepsilon},\mathbf{D}) = \frac{1}{2}\boldsymbol{\varepsilon}^{\mathrm{t}}\mathbf{c}^D\boldsymbol{\varepsilon} - \boldsymbol{\varepsilon}^{\mathrm{t}}\mathbf{h}^{\mathrm{t}}\mathbf{D} + \frac{1}{2}\mathbf{D}^{\mathrm{t}}\boldsymbol{\beta}^{\varepsilon}\mathbf{D}, \tag{7}$$

such that

$$\begin{aligned}&\boldsymbol{\sigma} = \partial H/\partial\boldsymbol{\varepsilon} = \mathbf{c}^D\boldsymbol{\varepsilon} - \mathbf{h}^{\mathrm{t}}\mathbf{D},\\ &\mathbf{E} = \partial H/\partial\mathbf{D} = -\mathbf{h}\boldsymbol{\varepsilon} + \boldsymbol{\beta}^{\varepsilon}\mathbf{D},\end{aligned} \tag{8}$$

where c_{ij}^D, h_{lj} and β_l^{ε} $(i,j = 1,...,6; l = 1,2,3)$ denote the elastic (for constant electric displacement), piezoelectric and dielectric (for constant strain) constants of the piezoelectric material, respectively.

For both extension and shear mode piezoelectric layers, only transverse electric field and displacements are considered ($D_1 = D_2 = 0$) since the layers have electrodes on top and bottom skins. However, faces and core layers are treated separately, since they have different poling directions. An additional assumption of plane stress state ($\sigma_3 = 0$) allows to write the following reduced constitutive equations for the faces and the core:

$$\begin{Bmatrix}\sigma_{1k}\\ E_{3k}\end{Bmatrix} = \begin{bmatrix}\bar{c}_{11}^{Dk} & -\bar{h}_{31}^k\\ -\bar{h}_{31}^k & \bar{\beta}_{33}^{\varepsilon k}\end{bmatrix}\begin{Bmatrix}\varepsilon_{1k}\\ D_{3k}\end{Bmatrix}, \tag{9}$$

and

$$\begin{Bmatrix}\sigma_{1c}\\ \sigma_{5c}\\ E_{3c}\end{Bmatrix} = \begin{bmatrix}\bar{c}_{33}^{Dc} & 0 & 0\\ 0 & c_{55}^{Dc} & -h_{15}^c\\ 0 & -h_{15}^c & \beta_{11}^{\varepsilon c}\end{bmatrix}\begin{Bmatrix}\varepsilon_{1c}\\ \varepsilon_{5c}\\ D_{3c}\end{Bmatrix}, \tag{10}$$

where,

$$\bar{c}_{11}^{Dk} = c_{11}^{Dk} - \frac{c_{13}^{Dk2}}{c_{33}^{Dk}},\ \bar{h}_{31}^k = h_{31}^k - h_{33}^k\frac{c_{13}^{Dk}}{c_{33}^{Dk}},\ \bar{\beta}_{33}^{\varepsilon k} = \beta_{33}^{\varepsilon k} + \frac{h_{33}^{k\ 2}}{c_{33}^{Dk}}, \tag{11}$$

$$\bar{c}_{33}^{Dc} = c_{33}^{Dc} - \frac{c_{13}^{Dc2}}{c_{11}^{Dc}}. \tag{12}$$

Finite element discretization

Lagrange linear shape functions are assumed for the axial displacements, u_t and u_b, and electric displacements in each layer, D_{3t}, D_{3c} and D_{3b}. For the transverse deflection w, Hermite cubic shape functions are assumed. These assumptions lead to a two node finite element with four mechanical dof and three electrical dof per node. The elementary mechanical degrees of freedom (dof) column vector $\mathbf{u}_n$ is defined as

$$\mathbf{u}_n = [u_t^{(1)}\ \ u_b^{(1)}\ \ w^{(1)}\ \ w'^{(1)}\ \ u_t^{(2)}\ \ u_b^{(2)}\ \ w^{(2)}\ \ w'^{(2)}]^{\mathrm{t}}. \tag{13}$$

The axial and transverse displacements of the face layers can be written in terms of the elementary dofs as

$$u_k = \mathbf{N}_{xk}\mathbf{u}_n,\ w = \mathbf{N}_z\mathbf{u}_n,\ k = t,b, \tag{14}$$

where

$$\begin{aligned}\mathbf{N}_{xt} &= \begin{bmatrix}N_1 & 0 & 0 & 0 & N_2 & 0 & 0 & 0\end{bmatrix},\\ \mathbf{N}_{xb} &= \begin{bmatrix}0 & N_1 & 0 & 0 & 0 & N_2 & 0 & 0\end{bmatrix},\\ \mathbf{N}_z &= \begin{bmatrix}0 & 0 & N_3 & N_4 & 0 & 0 & N_5 & N_6\end{bmatrix},\end{aligned} \tag{15}$$

and

$$N_1 = 1 - \frac{x}{L},\ N_2 = \frac{x}{L},\ N_3 = 1 - \frac{3x^2}{L^2} + \frac{2x^3}{L^3},\ N_4 = x\left(1 - \frac{x}{L}\right)^2,$$
$$N_5 = \frac{x^2}{L^2}\left(3 - \frac{2x}{L}\right),\ N_6 = \frac{x^2}{L}\left(\frac{x}{L} - 1\right). \tag{16}$$

The axial displacement of the core layer u_c and the cross-section rotations β_i can then be written, using $\beta_t = \beta_b = -w'$ and (2), as

$$u_c = \mathbf{N}_{xc}\mathbf{u}_n,\ \beta_i = \mathbf{N}_{ri}\mathbf{u}_n,\ i = t,c,b, \tag{17}$$

where

$$\mathbf{N}_{xc} = \frac{\mathbf{N}_{xt} + \mathbf{N}_{xb}}{2} + \frac{h_d}{4}\mathbf{N}'_z,\ \mathbf{N}_{rc} = \frac{\mathbf{N}_{xt} - \mathbf{N}_{xb}}{h_c} + \frac{h_m}{h_c}\mathbf{N}'_z,$$
$$\mathbf{N}_{rt} = \mathbf{N}'_{xt},\ \mathbf{N}_{rb} = \mathbf{N}'_{xb}. \tag{18}$$

According to expressions (5) and (6) for the generalized strains, ε_i^m, ε_i^f, and ε_i^c, they can be written in terms of the elementary dofs as

$$\varepsilon_i^m = \mathbf{B}_{mi}\mathbf{u}_n,\ \varepsilon_i^f = \mathbf{B}_{fi}\mathbf{u}_n,\ \varepsilon_c^c = \mathbf{B}_{cc}\mathbf{u}_n. \tag{19}$$

The membrane, bending and shear strain operators $\mathbf{B}_{mi}$, $\mathbf{B}_{fi}$ and $\mathbf{B}_{cc}$ are defined as

$$\mathbf{B}_{mi} = \mathbf{N}'_{xi},\ \mathbf{B}_{fi} = \mathbf{N}'_{ri},\ \mathbf{B}_{cc} = \mathbf{N}_{rc} + \mathbf{N}'_z. \tag{20}$$

The elementary electric dofs column vector $\mathbf{D}_n$ is defined as

$$\mathbf{D}_n = \begin{bmatrix} D_{3t}^{(1)} & D_{3c}^{(1)} & D_{3b}^{(1)} & D_{3t}^{(2)} & D_{3t}^{(2)} & D_{3b}^{(2)} \end{bmatrix}^{\mathrm{t}}. \tag{21}$$

Then, the electric displacement in the piezoelectric layers can be written in terms of the elementary dofs

$$D_{3i} = \mathbf{N}_{Di}\mathbf{D}_n,\ i = t,c,b, \tag{22}$$

where

$$\mathbf{N}_{Dt} = \begin{bmatrix} N_1 & 0 & 0 & N_2 & 0 & 0 \end{bmatrix},$$
$$\mathbf{N}_{Dc} = \begin{bmatrix} 0 & N_1 & 0 & 0 & N_2 & 0 \end{bmatrix}, \tag{23}$$
$$\mathbf{N}_{Db} = \begin{bmatrix} 0 & 0 & N_1 & 0 & 0 & N_2 \end{bmatrix}.$$

Variational formulation

The equation of motions can be written using the Hamilton's principle extended to piezoelectric media

$$\delta\Pi_b = \int_t \left[\sum_i (\delta T_i - \delta H_i) + \delta W_m\right] \mathrm{d}t = 0, \tag{24}$$

where δT_i, δH_i and δW_m are the virtual variations of kinetic energy T_i and electric enthalpy H_i of layer i and the total virtual work done by mechanical forces on the structure.

The virtual variation of kinetic energy for layer i of the sandwich beam can be written using the displacements fields defined in (1) and supposing that all layers are symmetric with respect to their neutral lines, $z = z_i$, such that integration over the cross-section areas leads to

$$\int_t \delta T_i \mathrm{d}t = -\int_t \int_0^L \left[\rho_i A_i \left(\delta u_i \ddot{u}_i + \delta w \ddot{w}\right) + \rho_i I_i \delta\beta_i \ddot{\beta}_i\right] \mathrm{d}x\, \mathrm{d}t, \tag{25}$$

where ρ_i is the mass density and A_i and I_i are the area and second moment of area of the cross-section of layer i, respectively, and the dot stands for time derivation.

Using the finite element discretization of generalized displacements (14) and (17),

$$\int_t \delta T_i \mathrm{d}t = -\int_t \delta\mathbf{u}_n^{\mathrm{t}} \mathbf{M}_i \ddot{\mathbf{u}}_n\, \mathrm{d}t, \tag{26}$$

where $\mathbf{M}_i$ is mass matrix of the layer i defined as

$$\mathbf{M}_i = \int_0^L \left[\rho_i A_i (\mathbf{N}_{xi}^{\mathrm{t}}\mathbf{N}_{xi} + \mathbf{N}_{zi}^{\mathrm{t}}\mathbf{N}_{zi}) + \rho_i I_i \mathbf{N}_{ri}^{\mathrm{t}}\mathbf{N}_{ri}\right] \mathrm{d}x. \tag{27}$$

The virtual variation of the electric enthalpy H_i for each layer will be composed of mechanical δH_{mi}, electromechanical (piezoelectric) δH_{mei}, and dielectric δH_{ei} contributions. In what follows, these are detailed for the faces $i = t,b$ and core $i = c$ layer.

For the core layer, both normal and shear strains contribute to the virtual variation of electric enthalpy, while for the faces only normal strains are relevant. Then, using (4) and supposing symmetric layers, the integration over the cross-section reduces δH_{mi} to

$$\delta H_{mk} = \int_0^L \left(\delta\varepsilon_k^m \bar{c}_{11}^{Dk} A_k \varepsilon_k^m + \delta\varepsilon_k^f \bar{c}_{11}^{Dk} I_k \varepsilon_k^f\right) \mathrm{d}x,\ k = t,b,$$
$$\delta H_{mc} = \int_0^L \left(\delta\varepsilon_c^m \bar{c}_{33}^{Dc} A_c \varepsilon_c^m + \delta\varepsilon_c^f \bar{c}_{33}^{Dc} I_c \varepsilon_c^f + \delta\varepsilon_c^c k_c c_{55}^{Dc} A_c \varepsilon_c^c\right) \mathrm{d}x, \tag{28}$$

where k_c is a shear correction factor for the Timoshenko core layer.

Also supposing symmetric layers and integrating in the cross-section, the piezoelectric contributions to the virtual variation of electric enthalpy can be written as

$$\delta H_{mek} = -\int_0^L \left(\delta\varepsilon_k^m \bar{h}_{31}^k A_k D_{3k} + \delta D_{3k} \bar{h}_{31}^k A_k \varepsilon_k^m\right) \mathrm{d}x,$$
$$\delta H_{mec} = -\int_0^L \left(\delta\varepsilon_c^c h_{15}^c A_c D_{3c} + \delta D_{3c} h_{15}^c A_c \varepsilon_c^c\right) \mathrm{d}x. \tag{29}$$

Notice that the piezoelectric effect couples the transversal electric displacement D_{3i} with membrane and bending strains ε_k^m and ε_k^f, for the faces, and with shear strain ε_c^c, for the core.

The dielectric contribution to the virtual variation of electric enthalpy can be written as

$$\delta H_{ek} = \int_0^L \delta D_{3k} \bar{\beta}_{33}^{\varepsilon k} A_k D_{3k} \mathrm{d}x, \quad \delta H_{ec} = \int_0^L \delta D_{3c} \beta_{11}^{\varepsilon c} A_c D_{3c} \mathrm{d}x. \tag{30}$$

The mechanical, piezoelectric and dielectric contributions to the virtual variation of electric enthalpy can be written in a discrete

form substituting the discretized generalized strains (19) and electric displacements (22) in equations (28), (29) and (30), such that

$$\begin{aligned} &\delta H_{mi} = \delta \mathbf{u}_n^{\mathrm{t}} \mathbf{K}_{mi} \mathbf{u}_n,\ \delta H_{mei} = -\delta \mathbf{u}_n^{\mathrm{t}} \mathbf{K}_{mei} \mathbf{D}_n - \delta \mathbf{D}_n^{\mathrm{t}} \mathbf{K}_{mei}^{\mathrm{t}} \mathbf{u}_n, \\ &\delta H_{ei} = \delta \mathbf{D}_n^{\mathrm{t}} \mathbf{K}_{ei} \mathbf{D}_n, \end{aligned} \tag{31}$$

where $\mathbf{K}_{mi}$ are the elastic stiffness matrices of the layer i written as

$$\begin{aligned} \mathbf{K}_{mk} &= \int_0^L \left(\mathbf{B}_{mk}^{\mathrm{t}} \bar{c}_{11}^{Dk} A_k \mathbf{B}_{mk} + \mathbf{B}_{fk}^{\mathrm{t}} \bar{c}_{11}^{Dk} I_k \mathbf{B}_{fk} \right) \mathrm{d}x, \\ \mathbf{K}_{mc} &= \int_0^L \left(\mathbf{B}_{mc}^{\mathrm{t}} \bar{c}_{33}^{Dc} A_c \mathbf{B}_{mc} + \mathbf{B}_{fc}^{\mathrm{t}} \bar{c}_{33}^{Dc} I_c \mathbf{B}_{fc} + \mathbf{B}_{cc}^{\mathrm{t}} k_c c_{55}^{Dc} A_c \mathbf{B}_{cc} \right) \mathrm{d}x, \end{aligned} \tag{32}$$

$\mathbf{K}_{mei}$ states for the electromechanical (piezoelectric) stiffness matrices

$$\begin{aligned} \mathbf{K}_{mek} &= \int_0^L \left(\mathbf{B}_{mk}^{\mathrm{t}} \bar{h}_{31}^{k} A_k \mathbf{N}_{Dk} \right) \mathrm{d}x, \\ \mathbf{K}_{mec} &= \int_0^L \left(\mathbf{B}_{cc}^{\mathrm{t}} h_{15} A_c \mathbf{N}_{Dc} \right) \mathrm{d}x, \end{aligned} \tag{33}$$

and $\mathbf{K}_{ei}$ are the dielectric stiffness matrices

$$\begin{aligned} \mathbf{K}_{ek} &= \int_0^L \left(\mathbf{N}_{Dk}^{\mathrm{t}} \bar{\beta}_{33}^{\varepsilon k} A_k \mathbf{N}_{Dk} \right) \mathrm{d}x, \\ \mathbf{K}_{ec} &= \int_0^L \left(\mathbf{N}_{Dc}^{\mathrm{t}} \beta_{11}^{\varepsilon c} A_c \mathbf{N}_{Dc} \right) \mathrm{d}x. \end{aligned} \tag{34}$$

The virtual work done by external mechanical forces can be written in terms of a vector of generalized mechanical forces $\mathbf{F}$ such that

$$\delta W_m = \delta \mathbf{u}_n^{\mathrm{t}} \mathbf{F}. \tag{35}$$

Replacing the discretized virtual work expressions in the Hamilton's principle (24) and assembling for all finite elements in the structure, the global equations of motion can be expressed as

$$\begin{bmatrix} \mathbf{M} & 0 \\ 0 & 0 \end{bmatrix} \begin{Bmatrix} \ddot{\mathbf{u}} \\ \ddot{\mathbf{D}} \end{Bmatrix} + \begin{bmatrix} \mathbf{K}_m & -\mathbf{K}_{me} \\ -\mathbf{K}_{me}^{\mathrm{t}} & \mathbf{K}_e \end{bmatrix} \begin{Bmatrix} \mathbf{u} \\ \mathbf{D} \end{Bmatrix} = \begin{Bmatrix} \mathbf{F} \\ 0 \end{Bmatrix}, \tag{36}$$

where $\mathbf{u}$ and $\mathbf{D}$ are the global mechanical and electric dofs and the mass and stiffness matrices and mechanical force vector were assembled for all layers and all finite elements.

Connecting Piezoelectric Patches to Electrodes and Electric Circuits

To account for the electrodes fully covering the piezoelectric patches top and bottom skins, the electric displacements of selected nodes and layers are set to be equal. This dof assignment can be represented by the following expression:

$$\mathbf{D} = \mathbf{L}_p \mathbf{D}_p\ ,\ \mathbf{D}_p = \begin{bmatrix} D_{p1} & D_{p2} & \cdots & D_{pn} \end{bmatrix}^{\mathrm{t}} \tag{37}$$

where $\mathbf{L}_p$ is a binary matrix and $\mathbf{D}_p$ is a vector of the electric displacement for one piezoelectric patch (constant throughout the electrode surface). Substituting (37) into the variational form of (36), the equations of motion are reduced to

$$\begin{bmatrix} \mathbf{M} & 0 \\ 0 & 0 \end{bmatrix} \begin{Bmatrix} \ddot{\mathbf{u}} \\ \ddot{\mathbf{D}}_p \end{Bmatrix} + \begin{bmatrix} \mathbf{K}_m & -\bar{\mathbf{K}}_{me} \\ -\bar{\mathbf{K}}_{me}^{\mathrm{t}} & \bar{\mathbf{K}}_e \end{bmatrix} \begin{Bmatrix} \mathbf{u} \\ \mathbf{D}_p \end{Bmatrix} = \begin{Bmatrix} \mathbf{F} \\ 0 \end{Bmatrix}, \tag{38}$$

where

$$\bar{\mathbf{K}}_{me} = \mathbf{K}_{me} \mathbf{L}_p\ ,\ \bar{\mathbf{K}}_e = \mathbf{L}_p^{\mathrm{t}} \mathbf{K}_e \mathbf{L}_p. \tag{39}$$

In addition, it is supposed that each piezoelectric actuator/sensor can be connected to an electric circuit composed of an inductance L_{cj}, a resistance R_{cj} and a voltage source V_{cj} in series, with $j = 1, ..., n$ where n is the number of electric circuits. The equations of motion for the circuits can be written using the Hamilton's principle also as

$$\delta \Pi_c = \int_t \sum_{j=1}^{n} \left(\delta T_{cj} + \delta W_{rj} + \delta W_{ej} \right) \mathrm{d}t = 0 \tag{40}$$

where δT_{cj}, δW_{rj} and δW_{ej} are, respectively, the virtual variation of the kinetic energy due to the inductances L_{cj} and the virtual work done by the resistances R_{cj} and voltage sources V_{cj} connected in series for the j-th electric circuit. These are written as

$$\begin{aligned} &\int_t \delta T_{cj}\ \mathrm{d}t = -\int_t \delta q_{cj}^{\mathrm{t}} L_{cj} \ddot{q}_{cj}\ \mathrm{d}t,\ \delta W_{rj} = -\delta q_{cj}^{\mathrm{t}} R_{cj} \dot{q}_{cj}, \\ &\delta W_{ej} = \delta q_{cj}^{\mathrm{t}} V_{cj},\ j = 1, \ldots, n. \end{aligned} \tag{41}$$

To account for the connection between piezoelectric patches and electric circuits, it is supposed that electric charges entering a given electric circuit are equal to electric charges of a given piezoelectric patch. Since, due to equipotentiality condition in the electrodes, the electric displacement is constant throughout the electrode surface, the electric charges for a given piezoelectric patch is obtained by multiplying the electric displacement by the electrode area. Thus, a diagonal matrix $\mathbf{A}_p$ with elements that are the electrodes areas of each piezoelectric patch is defined. Then, the vector of electric charges generated at the piezoelectric patches and, thus, entering the n electric circuits can be written as

$$\mathbf{q}_c = \mathbf{A}_p \mathbf{D}_p \tag{42}$$

Including the virtual works of (41) in the variational form of the equations of motion (38) leads to

$$\begin{aligned} \delta \mathbf{u}^{\mathrm{t}} \left(\mathbf{M}\ddot{\mathbf{u}} + \mathbf{K}_m \mathbf{u} - \bar{\mathbf{K}}_{me} \mathbf{D}_p - \mathbf{F} \right) + \delta \mathbf{D}_p^{\mathrm{t}} \left(-\bar{\mathbf{K}}_{me}^{\mathrm{t}} \mathbf{u} + \bar{\mathbf{K}}_e \mathbf{D}_p \right) \\ + \delta \mathbf{q}_c^{\mathrm{t}} \left(-\mathbf{L}_c \ddot{\mathbf{q}}_c - \mathbf{R}_c \dot{\mathbf{q}}_c + \mathbf{V}_c \right) = 0. \end{aligned} \tag{43}$$

Accounting for the relation between circuits' electric charges and patches' electric displacements (42), the structure-patches-circuits coupled equations of motion can then be written as

$$\begin{aligned} &\begin{bmatrix} \mathbf{M} & 0 \\ 0 & \mathbf{M}_q \end{bmatrix} \begin{Bmatrix} \ddot{\mathbf{u}} \\ \ddot{\mathbf{D}}_p \end{Bmatrix} + \begin{bmatrix} \mathbf{C} & 0 \\ 0 & \mathbf{C}_q \end{bmatrix} \begin{Bmatrix} \dot{\mathbf{u}} \\ \dot{\mathbf{D}}_p \end{Bmatrix} \\ &\qquad + \begin{bmatrix} \mathbf{K}_m & -\bar{\mathbf{K}}_{me} \\ -\bar{\mathbf{K}}_{me}^{\mathrm{t}} & \bar{\mathbf{K}}_e \end{bmatrix} \begin{Bmatrix} \mathbf{u} \\ \mathbf{D}_p \end{Bmatrix} = \begin{Bmatrix} \mathbf{F} \\ \mathbf{F}_q \end{Bmatrix}, \end{aligned} \tag{44}$$

where $\mathbf{M}_q = \mathbf{A}_p^{\mathrm{t}} \mathbf{L}_c \mathbf{A}_p$, $\mathbf{C}_q = \mathbf{A}_p^{\mathrm{t}} \mathbf{R}_c \mathbf{A}_p$, $\mathbf{F}_q = \mathbf{A}_p^{\mathrm{t}} \mathbf{V}_c$ and a structural damping matrix $\mathbf{C}$ can be added a posteriori.

Passive and Active Vibration Control Design

From (44), it is possible to observe that the shunt circuit can affect the structural response either passively through coupling of the dynamics of circuit and structure, via the piezoelectric patches, or actively through the application of an electric voltage in the circuit which excites the structure, also via the piezoelectric patches. These effects can be better observed in a frequency response function (FRF) of the structure when subjected to a mechanical or electrical excitation.

For a purely mechanical excitation, such that $V_c = 0$ and $\mathbf{F} = \mathbf{b}\tilde{f}e^{\mathrm{j}\omega t}$, the amplitude of a displacement output $y = \mathbf{cu}$ can be written such that $\tilde{y} = G_p(\omega)\tilde{f}$, where the FRF $G_p(\omega)$ is

$$G_p(\omega) = \mathbf{c}\big\{-\omega^2\mathbf{M} + \mathrm{j}\omega\mathbf{C} + \mathbf{K}_m - \bar{\mathbf{K}}_{me}(-\omega^2\mathbf{M}_q + \mathrm{j}\omega\mathbf{C}_q + \bar{\mathbf{K}}_e)^{-1}\bar{\mathbf{K}}_{me}^{\mathrm{t}}\big\}^{-1}\mathbf{b}, \quad (45)$$

from which it is possible to notice that the resistance and inductance have the effect of changing the dynamic stiffness of the structure. Two particular cases of interest can be derived: i) open-circuit when $\mathbf{C}_q \to \infty$ and ii) short-circuit when $\mathbf{M}_q = \mathbf{C}_q = 0$, in which cases

$$\begin{aligned} G_p^{OC}(\omega) &= \mathbf{c}\left\{-\omega^2\mathbf{M} + \mathrm{j}\omega\mathbf{C} + \mathbf{K}_m\right\}^{-1}\mathbf{b}, \\ G_p^{SC}(\omega) &= \mathbf{c}\left\{-\omega^2\mathbf{M} + \mathrm{j}\omega\mathbf{C} + \mathbf{K}_m - \bar{\mathbf{K}}_{me}\bar{\mathbf{K}}_e^{-1}\bar{\mathbf{K}}_{me}^{\mathrm{t}}\right\}^{-1}\mathbf{b}. \end{aligned} \quad (46)$$

As expected, no structural modification is observed in the open-circuit case while, for the short-circuit case, the stiffness of the piezoelectric patches is reduced.

For a purely electric excitation using a single pair patch-circuit, such that $\mathbf{F} = 0$ and $V_c = \tilde{V}_c e^{\mathrm{j}\omega t}$, the FRF between the output y and the applied voltage V_c is such that $\tilde{y} = G_c(\omega)\tilde{V}_c$, where

$$G_c(\omega) = \mathbf{c}\big\{-\omega^2\mathbf{M} + \mathrm{j}\omega\mathbf{C} + \mathbf{K}_m - \bar{\mathbf{K}}_{me}(-\omega^2\mathbf{M}_q + \mathrm{j}\omega\mathbf{C}_q + \bar{\mathbf{K}}_e)^{-1}\bar{\mathbf{K}}_{me}^{\mathrm{t}}\big\}^{-1} \times \bar{\mathbf{K}}_{me}(-\omega^2\mathbf{M}_q + \mathrm{j}\omega\mathbf{C}_q + \bar{\mathbf{K}}_e)^{-1}\mathbf{A}_p^{\mathrm{t}} \quad (47)$$

In this case, the resistance and inductance of the electric circuit have two effects. The first is a modification on the dynamic stiffness of the structure as in the previous case. The second is a modification of amplitude of the equivalent force input induced in the structure by the applied voltage, which for a properly adjusted circuit can lead to a desirable amplification of the control authority of the pair patch-circuit. The particular case of a simple voltage actuator can be derived by making $\mathbf{M}_q = \mathbf{C}_q = 0$, for which

$$G_c^V(\omega) = \mathbf{c}\left\{-\omega^2\mathbf{M} + \mathrm{j}\omega\mathbf{C} + \mathbf{K}_m - \bar{\mathbf{K}}_{me}\bar{\mathbf{K}}_e^{-1}\bar{\mathbf{K}}_{me}^{\mathrm{t}}\right\}^{-1}\bar{\mathbf{K}}_{me}\bar{\mathbf{K}}_e^{-1}\mathbf{A}_p^{\mathrm{t}} \quad (48)$$

Passive vibration control using electromechanical vibration absorbers

Starting from the equations of motion (44) for the case of a single passive electric shunt circuit (RL) connected to a piezoelectric patch embedded in the structure, it is desired to apply the theory of dynamic vibration absorbers for a particular vibration mode of interest. Therefore, the structural response is approximated by the contribution of a single vibration mode of interest such that

$$\mathbf{u}(t) = \boldsymbol{\phi}_n\alpha_n(t), \quad (49)$$

where $\boldsymbol{\phi}_n$ and α_n are the vibration mode of interest and its corresponding modal displacement. Thus, neglecting the structural damping, the equations of motion for the resulting two degree of freedom system can be written as

$$\begin{aligned} \ddot{\alpha}_n + \omega_n^2\alpha_n - k_pD_p &= b_nf, \\ m_q\ddot{D}_p + c_q\dot{D}_p + k_eD_p - k_p\alpha_n &= 0, \end{aligned} \quad (50)$$

where $\boldsymbol{\phi}_n^{\mathrm{t}}\mathbf{M}\boldsymbol{\phi}_n = 1$, $\boldsymbol{\phi}_n^{\mathrm{t}}\mathbf{K}_m\boldsymbol{\phi}_n = \omega_n^2$, $k_p = \boldsymbol{\phi}_n^{\mathrm{t}}\bar{\mathbf{K}}_{me}$ and $b_n = \boldsymbol{\phi}_n^{\mathrm{t}}\mathbf{b}$.

Assuming a mechanical excitation through input f, the structural response measured by a displacement output $y = c_n\alpha_n$, where $c_n = \mathbf{c}\boldsymbol{\phi}_n$, can be written such that its amplitude is $\tilde{y} = G_p(\omega)\tilde{f}$, where the amplitude of the FRF $G_p(\omega)$ is

$$|G_p(\omega)| = c_nb_n\left[(-\omega^2m_q + k_e)^2 + (\omega c_q)^2\right]^{1/2} \times \Big\{[\omega^4m_q - \omega^2(k_e + m_q{\omega_n}^2) + k_e{\omega_n}^2 - {k_p}^2]^2 + [(-\omega^2 + {\omega_n}^2)\omega c_q]^2\Big\}^{-1/2}. \quad (51)$$

For limited values of c_q, $|G_p(\omega)|$ has an anti-resonance at a frequency equal to the resonance frequency of the electrical circuit, defined as $\omega_e = (k_e/m_q)^{1/2}$, which can be designed to match the structural resonance of interest ω_n. This leads to an expression for m_q, and thus for the inductance L_c, in terms of ω_n, such that

$$L_c = \frac{k_e}{\omega_n^2A_p^2}, \quad (52)$$

where A_p is the surface area of the electrode covering the piezoelectric patch connected to the circuit. From the theory of dynamic vibration absorbers, it is known that the anti-resonance is accompanied by two resonances which may have their amplitudes controlled by the electric circuit damping c_q. One strategy to design the damping parameter is to minimize the difference between the resonances and anti-resonance amplitudes. This can be done by first using $\lim_{c_q\to 0}|G_p(\omega)|^2 = \lim_{c_q\to\infty}|G_p(\omega)|^2$ to find the frequencies for which the amplitude is independent of damping parameter which are

$$\omega_{1,2}^2 = \frac{1}{2}\left[\omega_e^2 + \omega_n^2 \pm \sqrt{(\omega_e^2 - \omega_n^2)^2 + 2\omega_e^2(k_p^2/k_e)}\right]. \quad (53)$$

Equalizing the vibration amplitudes at one of these invariant frequencies ω_1 and at the anti-resonance frequency ω_n leads to an expression for the resistance R_c in terms of the equivalent coupling stiffness k_p, electrical stiffness k_e, surface area of the electrode A_p and structural resonance frequency of interest ω_n,

$$R_c = \frac{k_p\sqrt{2k_e}}{\omega_n^2A_p^2}. \quad (54)$$

Active vibration control using piezoelectric actuators and state feedback

A state feedback LQR (Linear Quadratic Regulator) optimal control is considered. For that, it is necessary to rewrite the equations of motion (44) in state space form, such that a vector of state variables $\mathbf{z}$ is defined, containing the modal displacements and velocities of a series of vibration modes of interest and the electric displacements of the piezoelectric patches and their time-derivatives. This leads to

$$\dot{\mathbf{z}} = \hat{\mathbf{A}}\mathbf{z} + \hat{\mathbf{B}}\mathbf{V}_c + \hat{\mathbf{B}}_f\mathbf{f}\ ,\ \mathbf{y} = \hat{\mathbf{C}}_y\mathbf{z}, \tag{55}$$

where

$$\mathbf{z} = \begin{bmatrix} \boldsymbol{\alpha} \\ \mathbf{D}_p \\ \dot{\boldsymbol{\alpha}} \\ \dot{\mathbf{D}}_p \end{bmatrix},\ \hat{\mathbf{A}} = \begin{bmatrix} \mathbf{0} & \mathbf{0} & \mathbf{I} & \mathbf{0} \\ \mathbf{0} & \mathbf{0} & \mathbf{0} & \mathbf{I} \\ -\boldsymbol{\Omega}^2 & \mathbf{K}_p & -\boldsymbol{\Lambda} & \mathbf{0} \\ \mathbf{M}_q^{-1}\mathbf{K}_p^{\mathrm{t}} & -\boldsymbol{\Omega}_e^2 & \mathbf{0} & -\boldsymbol{\Lambda}_e \end{bmatrix},$$
$$\hat{\mathbf{B}} = \begin{bmatrix} \mathbf{0} \\ \mathbf{0} \\ \mathbf{0} \\ \mathbf{M}_q^{-1}\mathbf{A}_p^{\mathrm{t}} \end{bmatrix},\ \hat{\mathbf{B}}_f = \begin{bmatrix} \mathbf{0} \\ \mathbf{0} \\ \mathbf{b}_\phi \\ \mathbf{0} \end{bmatrix},\ \hat{\mathbf{C}}_y = \begin{bmatrix} \mathbf{c}_\phi & \mathbf{0} & \mathbf{0} & \mathbf{0} \end{bmatrix}. \tag{56}$$

The modal displacements are such that $\mathbf{u} = \boldsymbol{\Phi}\boldsymbol{\alpha}$ and, for mass normalized vibration modes, $\boldsymbol{\Omega}^2 = \boldsymbol{\Phi}^{\mathrm{t}}\mathbf{K}_m\boldsymbol{\Phi}$ and $\boldsymbol{\Lambda} = \boldsymbol{\Phi}^{\mathrm{t}}\mathbf{C}\boldsymbol{\Phi}$. $\boldsymbol{\Omega}$ is a diagonal matrix which elements are the undamped natural frequencies of the structure with piezoelectric patches in open-circuit. $\boldsymbol{\Omega}_e^2 = \mathbf{M}_q^{-1}\bar{\mathbf{K}}_e$ and $\boldsymbol{\Lambda}_e = \mathbf{M}_q^{-1}\mathbf{C}_q$ are both diagonal matrices which elements stand, respectively, for the squared natural frequencies of the electric circuits and the ratio between the resistances and inductances ($\mathbf{M}_q^{-1}\mathbf{C}_q = \mathbf{L}_c^{-1}\mathbf{R}_c$). The electromechanical coupling stiffness matrix projected in the undamped modal basis is defined as $\mathbf{K}_p = \boldsymbol{\Phi}^{\mathrm{t}}\bar{\mathbf{K}}_{me}$. Input $\mathbf{b}$ and output $\mathbf{c}$ distribution vectors are also defined, with modal projections $\mathbf{b}_\phi = \boldsymbol{\Phi}^{\mathrm{t}}\mathbf{b}$ and $\mathbf{c}_\phi = \mathbf{c}\boldsymbol{\Phi}$, and $\mathbf{f}$ is a vector of the amplitudes of each mechanical force applied to the structure.

A linear state feedback for the applied voltages $\mathbf{V}_c$ is assumed such that $\mathbf{V}_c = -\mathbf{g}\mathbf{z} = -\mathbf{g}_{dm}\boldsymbol{\alpha} - \mathbf{g}_{de}\mathbf{D}_p - \mathbf{g}_{vm}\dot{\boldsymbol{\alpha}} - \mathbf{g}_{ve}\dot{\mathbf{D}}_p$, where $\mathbf{g}$ is a vector of control gains for each state variable. Therefore, the state space equation (55) becomes

$$\dot{\mathbf{z}} = (\hat{\mathbf{A}} - \hat{\mathbf{B}}\mathbf{g})\mathbf{z} + \hat{\mathbf{B}}_f\mathbf{f}\ ,\ \mathbf{y} = \hat{\mathbf{C}}_y\mathbf{z}. \tag{57}$$

For a single-input mechanical excitation f, the closed-loop or controlled amplitude of a single displacement output y can be written such that $\tilde{y} = G_h(\omega)\tilde{f}$, where the FRF $G_h(\omega)$ is

$$G_h(\omega) = \hat{\mathbf{C}}_y(\mathrm{j}\omega\mathbf{I} - \hat{\mathbf{A}} + \hat{\mathbf{B}}\mathbf{g})^{-1}\hat{\mathbf{B}}_f, \tag{58}$$

which can also be derived from the second order equations of motion projected into the undamped modal basis leading to

$$G_h(\omega) = \mathbf{c}_\phi\big\{-\omega^2\mathbf{I} + \mathrm{j}\omega(\boldsymbol{\Lambda} + \mathbf{K}_p\mathbf{D}_{cc}^{-1}\mathbf{A}_p^{\mathrm{t}}\mathbf{g}_{vm}) + [\boldsymbol{\Omega}^2 + \mathbf{K}_p\mathbf{D}_{cc}^{-1}(\mathbf{A}_p^{\mathrm{t}}\mathbf{g}_{dm} - \mathbf{K}_p^{\mathrm{t}})]\big\}^{-1}\mathbf{b}_\phi, \tag{59}$$

where the closed-loop dynamic stiffness of the electric circuit $\mathbf{D}_{cc}$ is

$$\mathbf{D}_{cc} = -\omega^2\mathbf{M}_q + \mathrm{j}\omega(\mathbf{C}_q + \mathbf{A}_p^{\mathrm{t}}\mathbf{g}_{ve}) + (\bar{\mathbf{K}}_e + \mathbf{A}_p^{\mathrm{t}}\mathbf{g}_{de}). \tag{60}$$

In this work, the control gain $\mathbf{g}$ is calculated using the standard optimal LQR control theory applied to a single-input/single-output case, that is, with only one active-passive patch-circuit pair for the control to minimize the vibration amplitude at one specific location of the structure, such that the following objective function is minimized:

$$J = \frac{1}{2}\int_0^\infty \left(\dot{y}^2 + rV_c^2\right)\,\mathrm{d}t, \tag{61}$$

where $\dot{y}$ is the velocity at one location of interest and V_c is the control voltage applied to the active-passive shunt circuit. The weighting factor r is automatically adjusted to guarantee a maximum control voltage of 200 V in all cases following an iterative routine proposed in (Trindade, Benjeddou and Ohayon, 1999).

Results and Discussion

In this section, the FRFs of two cantilever beam configurations, with extension and shear piezoceramics as shown in Figure 1, are analyzed in order to evaluate the APPN performance in terms of passive damping, control authority and active-passive damping. The extension and shear piezoceramics are made of PZT-5H material whose properties are: $\bar{c}_{11}^D = 97.767$ GPa, $\bar{c}_{33}^D = 119.71$ GPa, $c_{55}^D = 42.217$ GPa, $\rho = 7500$ kg m^{-3}, piezoelectric coupling constants $\bar{h}_{31} = -1.3520\ 10^9$ N C^{-1} and $h_{15} = 1.1288\ 10^9$ N C^{-1}, and dielectric constants $\bar{\beta}_{33}^\varepsilon = 57.830\ 10^6$ m F^{-1} and $\beta_{11}^\varepsilon = 66.267\ 10^6$ m F^{-1}. For the Aluminium beam, material properties are: Young's modulus 70.3 GPa and density 2710 kg m^{-3} and, for the foam, Young's modulus 35.3 MPa, shear modulus 12.7 MPa and density 32 kg m^{-3}. A viscous damping of 0.5% and a shear correction factor $k_c = 0.83$ were considered.

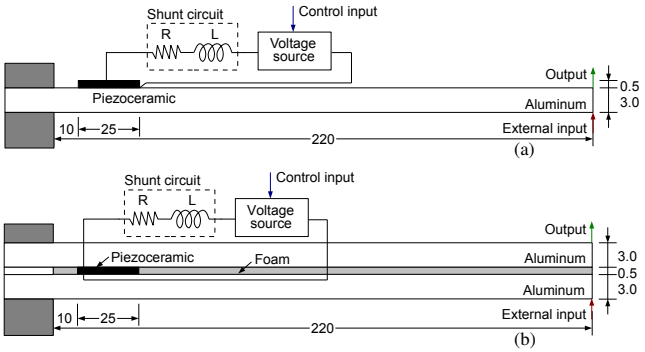

Figure 1. Representation of cantilever beams with piezoceramic patches: (a) in extension and (b) in shear.

First, the beam with extension piezoelectric patch is analyzed. The resistance and inductance were tuned to the first resonance frequency, using the methodology presented in the previous section. Notice, however, that the values obtained using (52) and (54), $R_c = 34117\ \Omega$ and $L_c = 406\ H$, are just a first approximation to the optimal values and had to be fine-tuned manually to $R_c = 31541\ \Omega$ and $L_c = 390\ H$. The purely passive action is obtained by eliminating the voltage source and the purely active action is obtained by making $R_c = L_c = 0$. For the general case, the inductance and resistance not only modify the dynamic stiffness of the structure, leading to damping and/or absorption, but also affects the active control authority of the actuator.

The purely passive performance of resistive and resonant shunt circuits can be evaluated using the frequency response of the beam tip

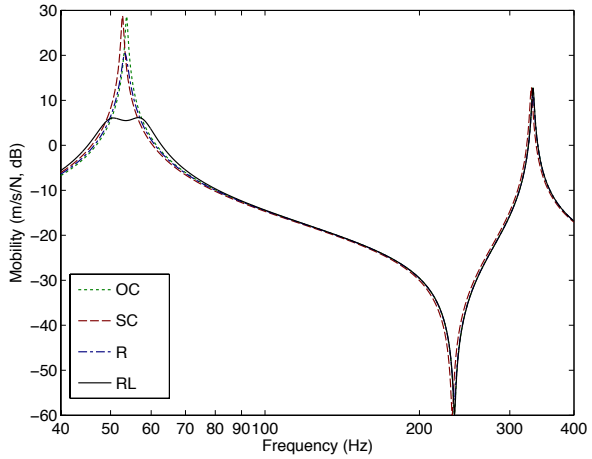

Figure 2. FRF of the beam with extension piezoceramic patch connected to a passive shunt circuit: G_p^{OC} (dotted), G_p^{SC} (dashed), G_p^{R} (dash-dot) and G_p^{RL} (solid).

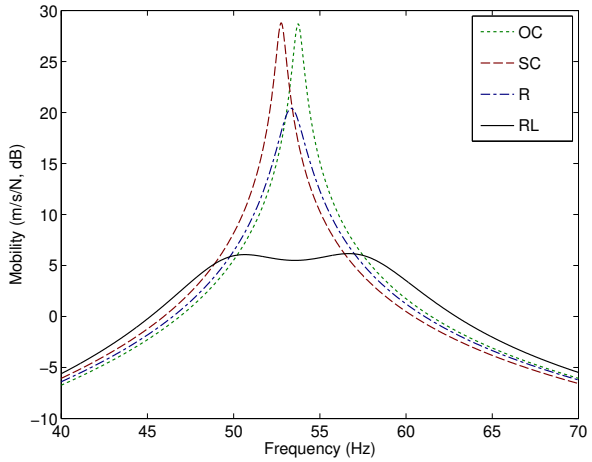

Figure 3. FRF, zoomed at the first resonance, of the beam with extension piezoceramic patch connected to a passive shunt circuit: G_p^{OC} (dotted), G_p^{SC} (dashed), G_p^{R} (dash-dot) and G_p^{RL} (solid).

velocity when the beam is subject to a transverse force at the same point (Figure 2). The reference is considered to be unitary. It is possible to observe that both shunt circuits affect significantly only the first resonance, as expected. Figure 3 presents the same response, zoomed at the first resonance, from which one can conclude that both shunt circuits may yield a vibration amplitude reduction but the resonant circuit leads to a much better performance (approximately 22 dB vibration amplitude reduction). The resistive circuit leads to a variation in the resonance frequency, between short-circuit and open-circuit ones, and also induces an equivalent damping factor. For the resonant circuit, tuning of its resistance allows to reduce amplitude at the structure's resonance frequency (i.e. the anti-resonance of the coupled system) at the cost of increasing the amplitude at the two resonance frequencies of the coupled system. Figure 4 shows the effect of increasing and decreasing the resistance of the optimal resonant circuit by 20%.

Figure 5 shows the active control authority of the piezoelectric material, acting as an actuator through the shunt circuit, measured as the beam tip velocity response when subject to a voltage applied to the circuit. As expected, the resistive shunt circuit diminishes the active control authority for all frequencies, since part of the input electric

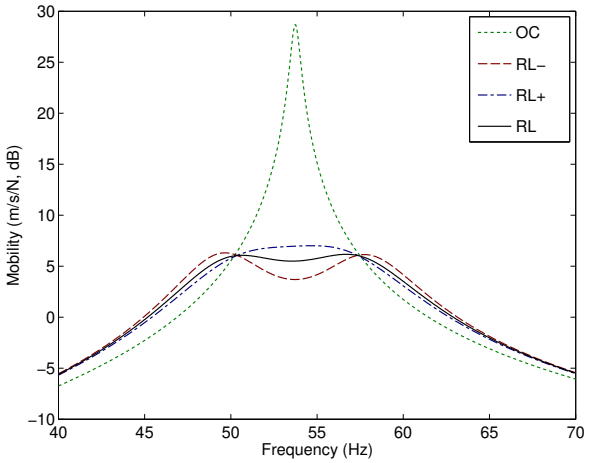

Figure 4. FRF of the beam with extension piezoceramic patch connected to a resonant circuit subject to variations in the resistance value: open-circuit G_p^{OC} (dotted), optimal RL G_p^{RL} (solid), RL with 20% reduction on resistance value G_p^{RL-} (dashed) and RL with 20% increase on resistance value G_p^{RL+} (dash-dot).

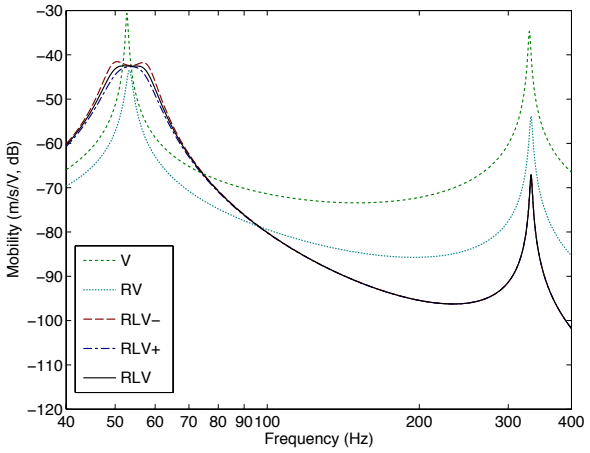

Figure 5. Control authority of the extension piezoceramic patch: without shunt G_c^{V} (dotted), resistive shunt G_c^{R} (fine dot), RL shunt with 20% reduction on resistance value G_c^{RL-} (dashed), RL shunt with 20% increase on resistance value G_c^{RL+} (dash-dot) and optimal RL shunt G_c^{RL} (solid).

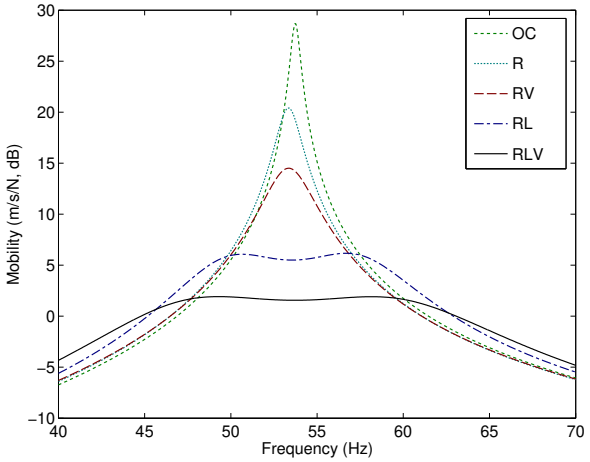

Figure 6. FRF of the beam with extension piezoceramic patch connected to passive and active-passive shunt circuits: open-circuit G_p^{OC} (dotted), passive R shunt G_p^{R} (fine dot), active-passive R shunt G_h^{R} (dashed), passive RL shunt G_p^{RL} (dash-dot) and active-passive RL shunt G_h^{RL} (solid).

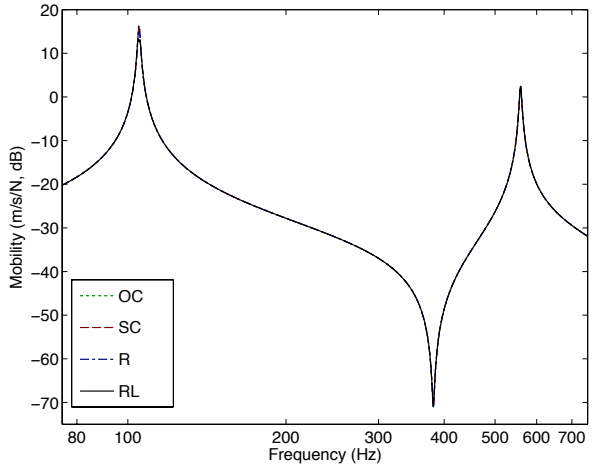

Figure 7. FRF of the beam with shear piezoceramic patch connected to a passive shunt circuit: G_p^{OC} (dotted), G_p^{SC} (dashed), G_p^{R} (dash-dot) and G_p^{RL} (solid).

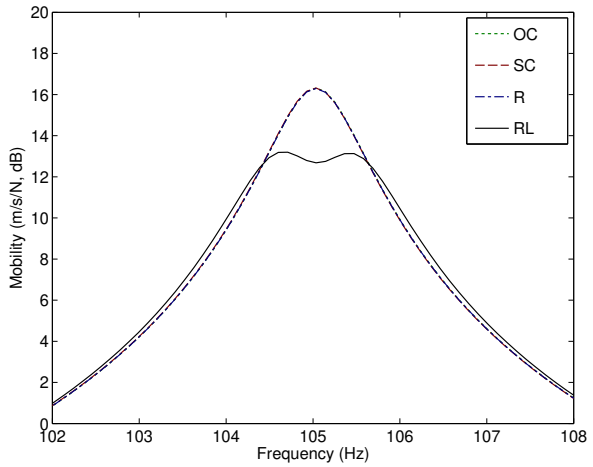

Figure 8. FRF, zoomed at the first resonance, of the beam with shear piezoceramic patch connected to a passive shunt circuit: G_p^{OC} (dotted), G_p^{SC} (dashed), G_p^{R} (dash-dot) and G_p^{RL} (solid).

energy is being dissipated through the resistance. On the other hand, the resonant shunt circuit allows an increase of the active control authority around the first resonance at the cost of reducing it for the remaining frequency range.

Then, the LQR state feedback control strategy voltage presented previously was considered to evaluate the control voltage to be applied to the circuit and actively reduce the vibration amplitude of the beam. Figure 6 shows the beam tip mobility, zoomed at the first resonance, for uncontrolled beam (open-circuit, $R_c \rightarrow \infty$), passive controlled beam with resistive ($R_c = 144\ k\Omega,\ L_c = 0,\ V_c = 0$) and resonant ($R_c = 31541\ \Omega,\ L_c = 390\ H,\ V_c = 0$) shunt circuits, and active-passive controlled beam with resistive ($R_c = 144\ k\Omega,\ L_c = 0,\ V_c < 200\ V$) and resonant ($R_c = 31541\ \Omega,\ L_c = 390\ H,\ V_c < 200\ V$) shunt circuits. The active-passive control yields better performance than its passive counterpart with amplitude reductions of approximately 14 dB (resistive) and 28 dB (resonant). Therefore, despite the small reduction on active control authority at the resonance frequency, active-passive control always outperforms the corresponding passive one.

Then, a similar analysis was performed for the sandwich beam with embedded shear piezoelectric patch. In this case, the resistance

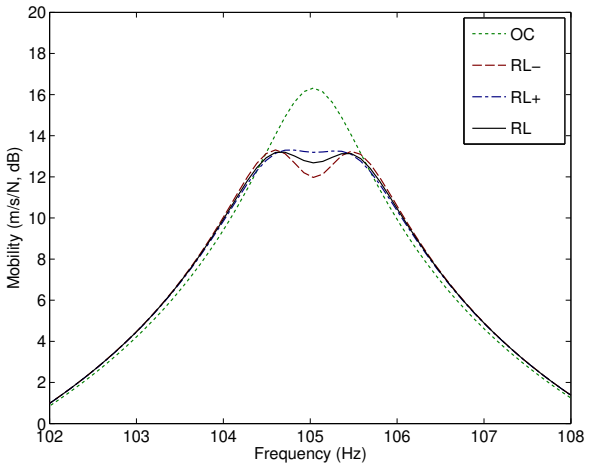

Figure 9. FRF of the beam with shear piezoceramic patch connected to a resonant circuit subject to variations in the resistance value: open-circuit G_p^{OC} (dotted), optimal RL G_p^{RL} (solid), RL with 20% reduction on resistance value G_p^{RL-} (dashed) and RL with 20% increase on resistance value G_p^{RL+} (dash-dot).

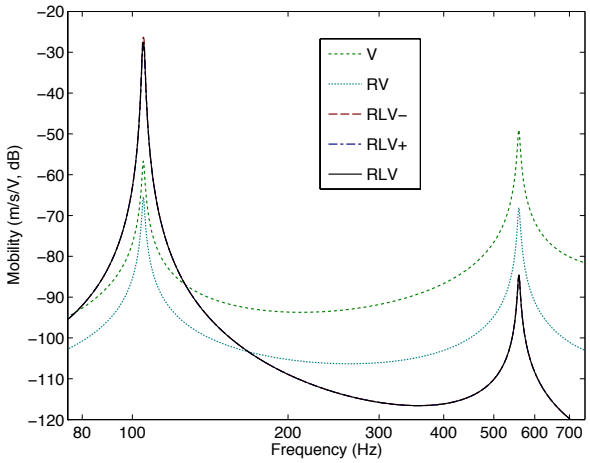

Figure 10. Control authority of the shear piezoceramic patch: without shunt G_c^{V} (dotted), resistive shunt G_c^{R} (fine dot), RL shunt with 20% reduction on resistance value G_c^{RL-} (dashed), RL shunt with 20% increase on resistance value G_c^{RL+} (dash-dot) and optimal RL shunt G_c^{RL} (solid).

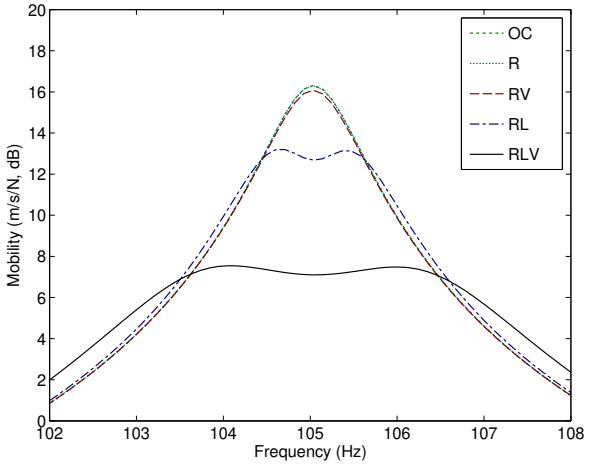

Figure 11. FRF of the beam with shear piezoceramic patch connected to passive and active-passive shunt circuits: open-circuit G_p^{OC} (dotted), passive R shunt G_p^{R} (fine dot), active-passive R shunt G_h^{R} (dashed), passive RL shunt G_p^{RL} (dash-dot) and active-passive RL shunt G_h^{RL} (solid).

and inductance values obtained from (52) and (54) are $R_c = 835.9\ \Omega$ and $L_c = 121.7\ H$ and were fine-tuned manually to $R_c = 835.8\ \Omega$ and $L_c = 121.5\ H$. The purely passive performance of resistive and resonant shunt circuits are presented in Figures 7 and 8. It is possible to observe that the vibration reduction performance is much smaller than in the previous case for both shunt circuits. This is due to the fact the sandwich design considered does not induce significant shear strains in the piezoelectric patch when the beam vibrates on the first mode. For the resonant circuit, the amplitude at structure's first resonance can be further reduced by decreasing the resistance of the circuit as can be seen in Figure 9, which shows the effect of increasing and decreasing the resistance of the optimal resonant circuit by 20%.

Figure 10 shows the active control authority of the shear piezoelectric patch, acting as an actuator through the shunt circuit, measured as the beam tip velocity response when subject to a voltage applied to the circuit. Here, the resistive shunt circuit also leads to a reduction on the active control authority for all frequencies. On the other hand, the resonant shunt circuit yields a very large increase on the active control authority around the first resonance. This fact indicates that, although the passive performance of the shear configuration is not very good, it might be an adequate choice for active or active-passive control since its control authority can be significantly enhanced by the circuit tuning. Indeed, as shown in Figure 11, when applying a similar LQR control strategy to the sandwich beam with shear actuator, the vibration amplitude is greatly reduced as compared to the corresponding passive case. As for the previous case, Figure 11 compares the frequency response of the beam when uncontrolled (open-circuit, $R_c \to \infty$), passive controlled with resistive ($R_c = 593\ k\Omega,\ L_c = 0,\ V_c = 0$) and resonant ($R_c = 835.8\ \Omega,\ L_c = 121.5\ H,\ V_c = 0$) shunt circuits, and active-passive controlled with resistive ($R_c = 593\ k\Omega,\ L_c = 0,\ V_c < 200\ V$) and resonant ($R_c = 835.8\ \Omega,\ L_c = 121.5\ H,\ V_c < 200\ V$) shunt circuits. The shear active-passive resonant control leads to an amplitude reduction of approximately 10 dB.

Stochastic Modeling for Uncertainties Analysis

This section presents an approach for analyzing random uncertainties for the resistance R and inductance L elements of the electric shunt circuits. An appropriate probabilistic model for each random variable, $\widehat{R}$ and $\widehat{L}$, is constructed accounting for the available information only, which is the following: (1) the support of the probability density function is $]0,+\infty[$; (2) the mean values are such that $E[R] = \underline{R}$ and $E[L] = \underline{L}$; and (3) zero is a repulsive value for the positive-valued random variables which is accounted for by the condition $E[ln(R)] = c_R$ with $|c_R| < +\infty$ and $E[ln(L)] = c_L$ with $|c_L| < +\infty$. Therefore, the Maximum Entropy Principle yields the following Gamma probability density functions for R and L (Soize, 2001; Cataldo et al., 2009; Ritto et al., 2010)

$$p_R(R) = \mathbb{I}_{]0,+\infty[}(R)\frac{1}{\underline{R}}\left(\frac{1}{\delta_R^2}\right)^{\delta_R^{-2}}\frac{1}{\Gamma(\delta_R^{-2})}\left(\frac{R}{\underline{R}}\right)^{\delta_R^{-2}-1}\exp\left(-\frac{R}{\delta_R^2\underline{R}}\right) \tag{62}$$

and

$$p_L(L) = \mathbb{I}_{]0,+\infty[}(L)\frac{1}{\underline{L}}\left(\frac{1}{\delta_L^2}\right)^{\delta_L^{-2}}\frac{1}{\Gamma(\delta_L^{-2})}\left(\frac{L}{\underline{L}}\right)^{\delta_L^{-2}-1}\exp\left(-\frac{L}{\delta_L^2\underline{L}}\right) \tag{63}$$

in which $\delta_R = \sigma_R/\underline{R}$ and $\delta_L = \sigma_L/\underline{L}$ are the relative dispersions of $\widehat{R}$ and $\widehat{L}$ and σ_R and σ_L are their standard deviations. The Gamma function is defined as $\Gamma(\alpha) = \int_0^\infty t^{\alpha-1}e^{-t}\mathrm{d}t$. These probability density functions are shown in Figure 12 together with the histograms of random sets for R and L generated with MATLAB function *gamrnd*, considering 10000 realizations. The vectors of random realizations for $\widehat{R}$ and $\widehat{L}$ where then combined into pairs of RL parameters, which were then applied to the evaluation of realizations of the FRF $G_p(\theta_j,\omega)$, $G_c(\theta_j,\omega)$ and $G_h(\theta_j,\omega)$ using equations (45), (47) and (58), respectively. To improve the analysis of the sensitiveness of the responses to the circuit parameters, three values were considered for the relative dispersions δ_R and δ_L: 5%, 10% and 20%. The mean-square convergence analysis with respect to the independent realizations of random variable $\widehat{G}_p(\omega)$, denoted by $G_p(\theta_j,\omega)$ was carried out considering the function

$$conv(n_s) = \frac{1}{n_s}\sum_{j=1}^{n_s}\int \|G_p(\theta_j,\omega) - G_p^N(\omega)\|^2\,\mathrm{d}\omega, \tag{64}$$

where n_s is the number of simulations, or the number of RL pairs considered, and $G_p^N(\omega)$ is the response calculated using the corresponding mean model. Figure 13 shows the mean-square convergence analysis for extension and shear configurations considering $\delta_R = \delta_L = 0.10$. It is possible to observe that for both cases 3000 simulations are enough to assure convergence. Despite that, the statistical analyses presented in the following sections consider all 10000 simulations performed.

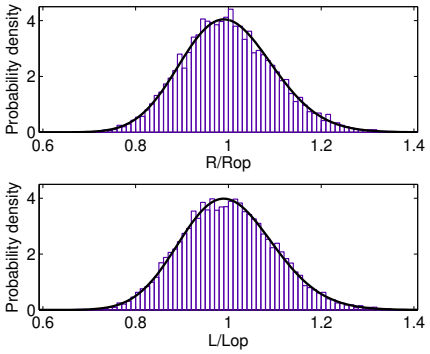

Figure 12. Probability density function for resistance (R/Rop) and inductance (L/Lop) values.

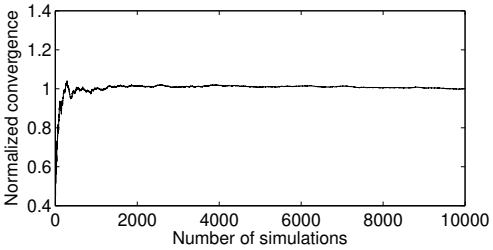

Figure 13. Mean square convergence of Monte Carlo simulation.

The statistical analyses of the FRF amplitudes were performed using their 10000 realizations at each frequency to calculate the corresponding mean values and 95% confidence intervals. The 95% confidence intervals were evaluated using the 2.5% and 97.5% percentiles of the realizations of FRF amplitudes at each frequency. Figure 14 summarizes the simulation procedure.

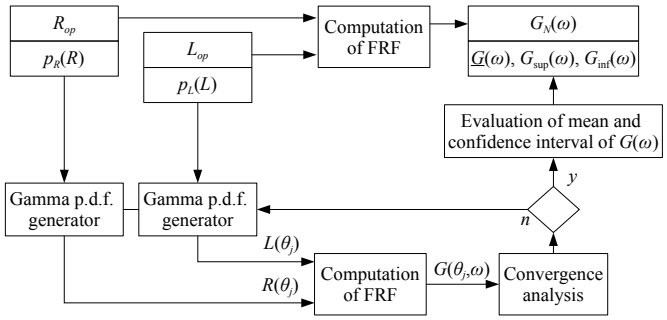

Figure 14. Schematic procedure for the computation of FRFs mean and confidence intervals.

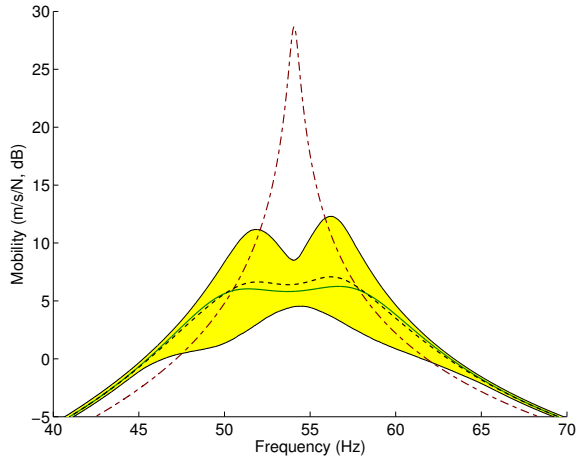

Figure 15. FRF of the beam with extension piezoceramic patch connected to a passive shunt circuit: G_p^{OC} (dash-dot), G_p^N (solid), $\underline{G}_p$ (dashed) and G_p^{CI} (filled) for $\delta_R = \delta_L = 0.10$.

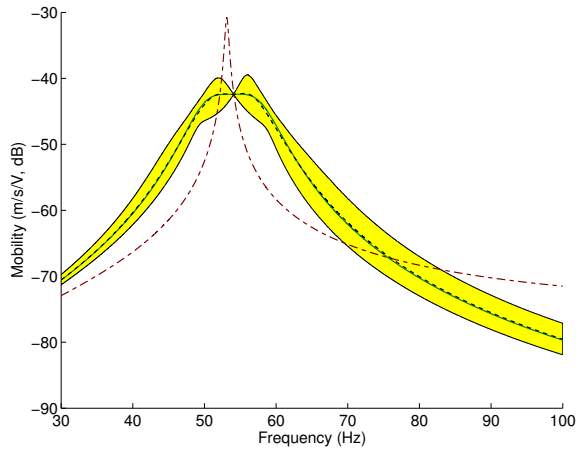

Figure 16. Control authority of the extension piezoceramic patch with and without shunt circuit: G_c^V (dash-dot), G_c^N (solid), $\underline{G}_c$ (dashed) and G_c^{CI} (filled) for $\delta_R = \delta_L = 0.10$.

Figure 15 shows the FRFs for the extension configuration with OC (G_p^{OC}) and RL shunted (G_p^N) piezoceramics, where, for last case, the nominal values of $R = 31541\ \Omega$ and $L = 390$ H were used. It also shows the mean value ($\underline{G}_p$) and 95% confidence intervals (G_p^{CI}) of random variable $\widehat{G}_p(\omega)$ for $\delta_R = \delta_L = 0.10$. Notice that the RL shunt circuit does not affect the FRF but near the first resonance (for which the shunt circuit was designed). In the FRF zoomed near the first resonance (Figure 15), one may notice that the nominal model

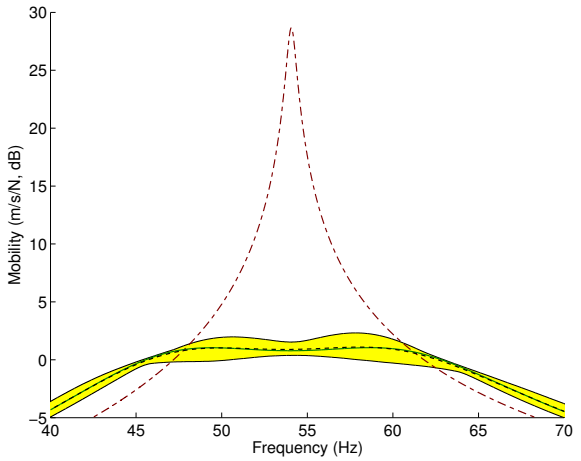

Figure 17. FRF of the beam with extension piezoceramic patch connected to an active-passive shunt circuit: G_h^{OC} (dash-dot), G_h^N (solid), $\underline{G}_h$ (dashed) and G_h^{CI} (filled) for $\delta_R = \delta_L = 0.10$.

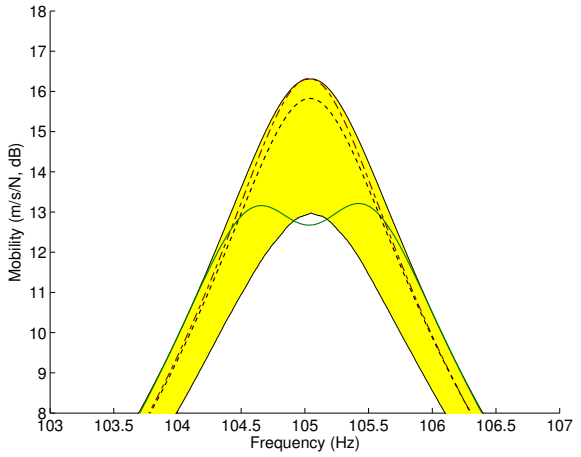

Figure 18. FRF of the beam with shear piezoceramic patch connected to a passive shunt circuit: G_p^{OC} (dash-dot), G_p^N (solid), $\underline{G}_p$ (dashed) and G_p^{CI} (filled) for $\delta_R = \delta_L = 0.10$.

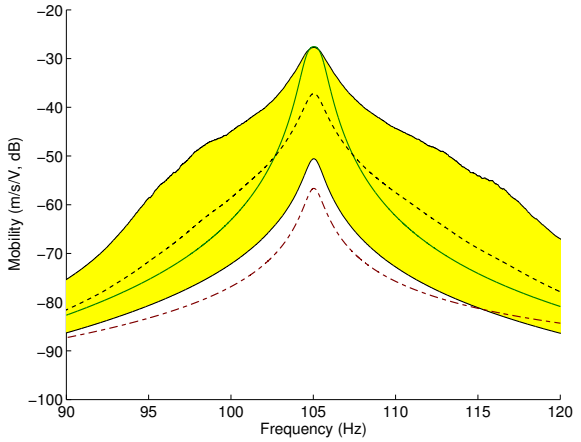

Figure 19. Control authority of the shear piezoceramic patch with and without shunt circuit: G_c^V (dash-dot), G_c^N (solid), $\underline{G}_c$ (dashed) and G_c^{CI} (filled) for $\delta_R = \delta_L = 0.10$.

indicates a reduction in the vibration amplitude of 22 dB (considering the difference between peak responses for OC and RL), while when considering the circuit components uncertainties this reduction is

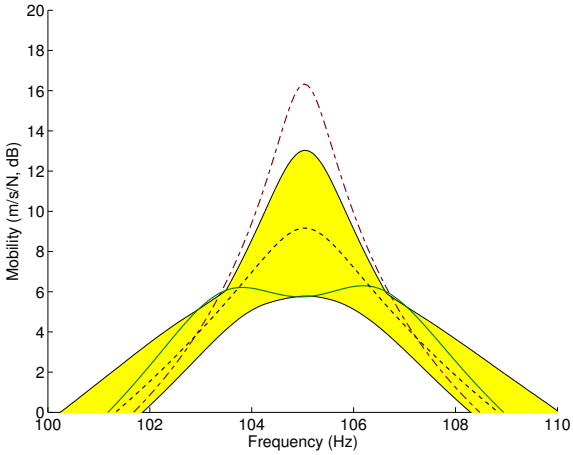

Figure 20. FRF of the beam with shear piezoceramic patch connected to an active-passive shunt circuit: G_h^{OC} (dash-dot), G_h^N (solid), $\underline{G}_h$ (dashed) and G_h^{CI} (filled) for $\delta_R = \delta_L = 0.10$.

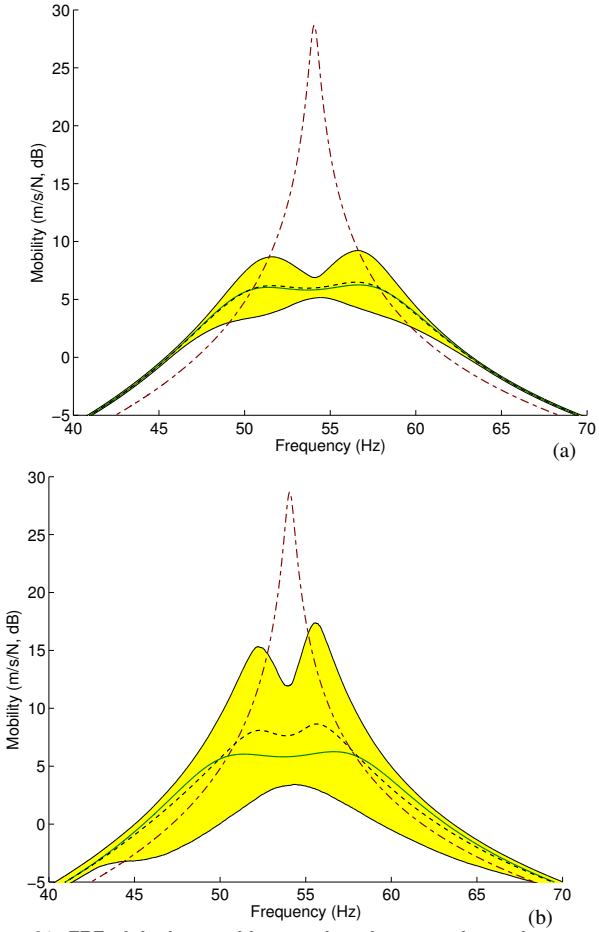

Figure 21. FRF of the beam with extension piezoceramic patch connected to a passive shunt circuit: G_p^{OC} (dash-dot), G_p^N (solid), $\underline{G}_p$ (dashed) and G_p^{CI} (filled) for: (a) $\delta_R = \delta_L = 0.05$ and (b) $\delta_R = \delta_L = 0.20$.

found to be in the range 16-24 dB. It can be also noticed that the difference between the mean and nominal FRFs is almost negligible.

Then, an analysis of the control authority FRFs for the extension configuration with purely active (G_c^V) and RL shunted (G_c^N) was performed, including its mean ($\underline{G}_c$) and 95% confidence intervals (G_c^{CI}) for $\delta_R = \delta_L = 0.10$. Figure 16 shows that despite the circuit

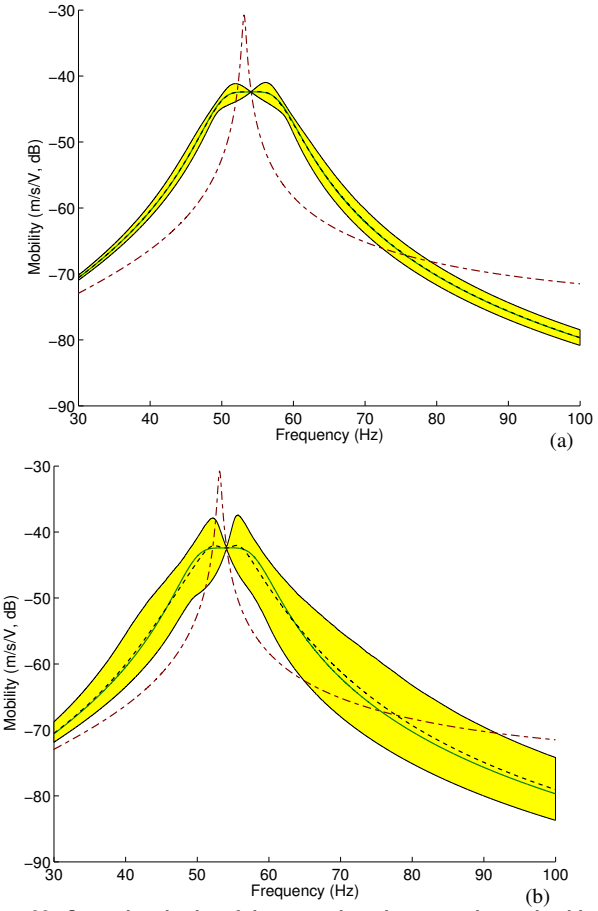

Figure 22. Control authority of the extension piezoceramic patch with and without shunt circuit: G_c^V (dash-dot), G_c^N (solid), $\underline{G}_c$ (dashed) and G_c^{CI} (filled) for: (a) $\delta_R = \delta_L = 0.05$ and (b) $\delta_R = \delta_L = 0.20$.

components uncertainties, the control authority is indeed increased near the first resonance at the cost of being significantly reduced for higher frequencies. The active-passive vibration control performance can be observed in Figure 17, which shows the FRFs for the uncontrolled (G_p^{OC}) and controlled structure (G_h^N), including its mean ($\underline{G}_h$) and confidence intervals (G_h^{CI}) for $\delta_R = \delta_L = 0.10$. Comparison with Figure 15 shows that the LQR control combined with the resonant shunt circuit allows to reduce further the vibration amplitude. Indeed, the nominal model indicates a reduction of 27.5 dB, while the confidence intervals indicate a reduction between 27 dB and 28 dB. It is also worthwhile to notice that the active control also shrinks the confidence intervals, compared to the passive case.

Similar analyses were done for the shear configuration. Hence, Figure 18 shows the FRFs with OC (G_p^{OC}) and RL shunted (G_p^N) piezoceramics. For the present shear case, the nominal values of $R = 835.8\ \Omega$ and $L = 121.5$ H were used. Figure 18 also shows the mean value ($\underline{G}_p$) and 95% confidence intervals (G_p^{CI}) for $\delta_R = \delta_L = 0.10$. In this case, a much smaller vibration amplitude reduction is observed, since the shear configuration is less appropriate to control the first vibration mode. The nominal model indicates a reduction of 3 dB and based on the 95% confidence intervals one could observe a reduction between 0 dB and 3.3 dB. Notice that, for this configuration, the anti-resonance observed in the nominal model is outside the confidence intervals. This is due to the fact that only the nearly perfect combination of optimal resistance and inductance values may lead to such performance. The shear configuration leads

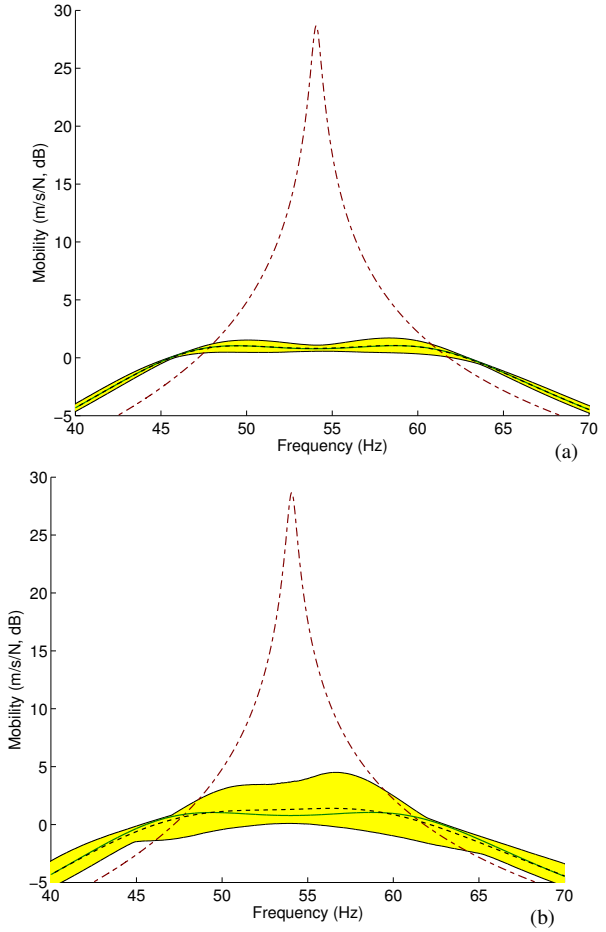

Figure 23. FRF of the beam with extension piezoceramic patch connected to an active-passive shunt circuit: G_h^{OC} (dash-dot), G_h^N (solid), $\underline{G}_h$ (dashed) and G_h^{CI} (filled) for: (a) $\delta_R = \delta_L = 0.05$ and (b) $\delta_R = \delta_L = 0.20$.

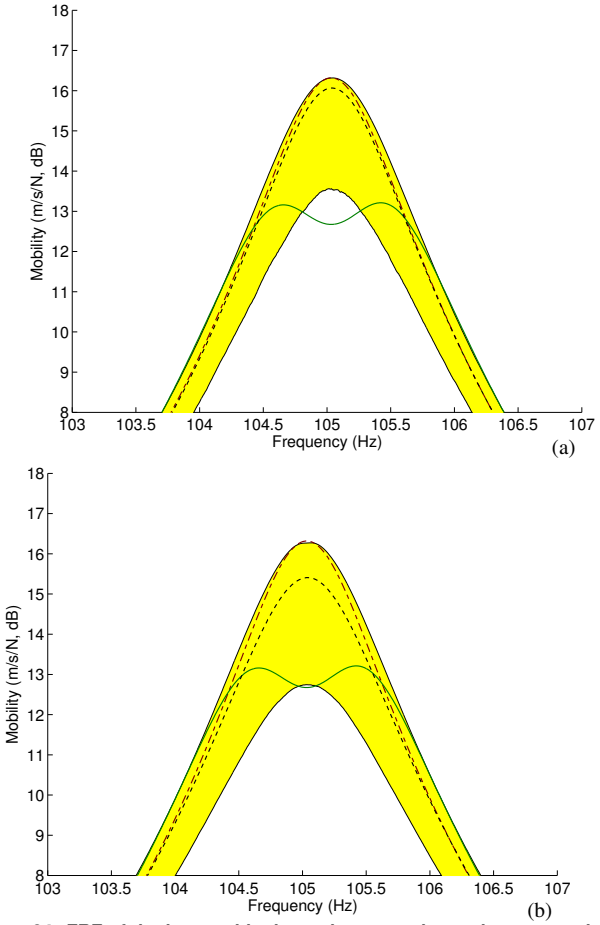

Figure 24. FRF of the beam with shear piezoceramic patch connected to a passive shunt circuit: G_p^{OC} (dash-dot), G_p^N (solid), $\underline{G}_p$ (dashed) and G_p^{CI} (filled) for: (a) $\delta_R = \delta_L = 0.05$ and (b) $\delta_R = \delta_L = 0.20$.

to a significant control authority amplification near the first resonance and, differently from the extension configuration, it occurs also at the resonance (Figure 19). This amplification leads to an increase of 29 dB at the resonance, according to the nominal model, and in the range $\{6\text{-}29\}$ dB, according to the 95% confidence intervals. From Figure 20, the vibration amplitude reduction induced by the active-passive control is 10 dB, according to the nominal model, and between 3 dB and 11 dB, according to the 95% confidence intervals.

It is also worthwhile to analyse the effect of the relative dispersions of resistance and inductance values on the confidence intervals of the responses of passive and active-passive controlled structures and the control authority of the shunted piezoelectric actuators. Therefore, two additional values for relative dispersions δ_R and δ_L were considered: 0.05 and 0.20. It is expected that higher relative dispersions would lead to wider confidence intervals and vice-versa. Figures 21, 22 and 23 show, respectively, the frequency responses G_p, G_c and G_h of the structure with the extension piezoceramics for the two additional relative dispersions. It can be observed in Figure 21, as expected, that the confidence interval is widened (shrunk) compared to the previous case (Figure 15) for larger (smaller) relative dispersions. The range of vibration amplitude reduction (considering the difference between peak responses) becomes 19-24 dB, for 5% relative dispersion, and 11-25 dB, for 20% relative dispersion. The same behaviour was observed for the control authority (Figure 22) and active-passive case (Figure 23). The range of vibration amplitude reduction when using the active-passive shunt circuit remains 27-28 dB, for 5% relative dispersion, and is widened to 24-29 dB, for 20% relative dispersion.

Similar behaviour was also observed in an analysis performed for the shear actuated sandwich beam. The range of vibration amplitude reduction for the beam with shear piezoceramic patch connected to a passive resonant shunt circuit was 0-2.7 dB and 0-3.6 dB for 5% and 20% relative dispersions, respectively (Figure 24). In terms of control authority, as shown in Figure 25, increasing the resistance and inductance relative dispersions yields decreasing lower limit for the confidence intervals, 16 dB and 0 dB for 5% and 20% relative dispersions, respectively, while the upper limit remains unchanged (29 dB). The confidence intervals for the active-passive performance, in terms of vibration amplitude reduction, of the shear actuated piezoceramics are also widened when increasing the corresponding resistance and inductance relative dispersions and vice-versa. The range of vibration amplitude reduction for the active-passive shunted shear piezoceramics is 5-11 dB, for 5% relative dispersion, and 2-11 dB, for 20% relative dispersion.

Concluding Remarks

This work presented an analysis of active-passive damping performance of beams with extension and shear active-passive piezoelectric networks (APPN). For that, a coupled finite element

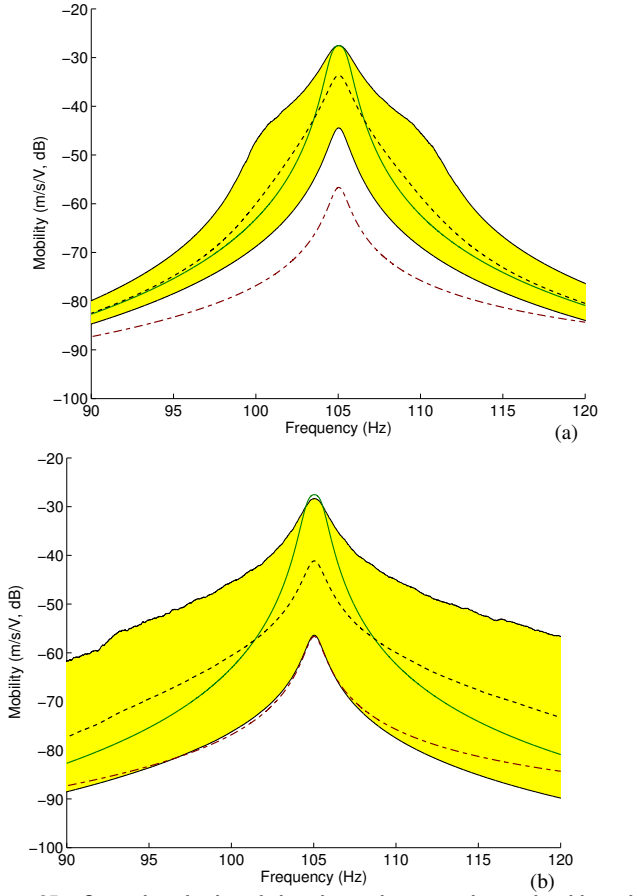

Figure 25. Control authority of the shear piezoceramic patch with and without shunt circuit: G_c^V (dash-dot), G_c^N (solid), $\underline{G}_c$ (dashed) and G_c^{CI} (filled) for: (a) $\delta_R = \delta_L = 0.05$ and (b) $\delta_R = \delta_L = 0.20$.

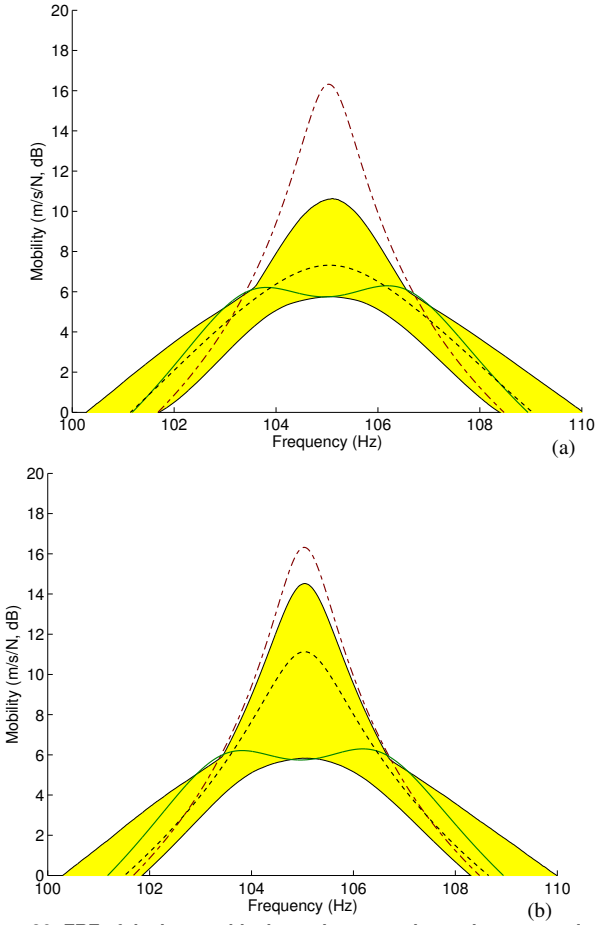

Figure 26. FRF of the beam with shear piezoceramic patch connected to an active-passive shunt circuit: G_h^{OC} (dash-dot), G_h^N (solid), $\underline{G}_h$ (dashed) and G_h^{CI} (filled) for: (a) $\delta_R = \delta_L = 0.05$ and (b) $\delta_R = \delta_L = 0.20$.

model with mechanical and electrical degrees of freedom was developed and used to design passive and active control parameters. Then, a stochastic modeling and analysis of two cantilever beam configurations, with extension and shear APPN, was performed to evaluate the effect of uncertainties in circuit components on passive and active-passive vibration control. Results have shown that active-passive shunt circuits can be very interesting since they may combine an adequate passive control performance with an increase of the active control authority when a control voltage is applied to the circuit. For the extension configuration, vibration amplitude reductions of up to 22 dB and 28 dB were obtained for the purely passive and active-passive cases, respectively. Considering relative dispersions of 10% for the resistance and inductance values, the passive and active-passive amplitude reductions were found to be in the ranges 16-24 dB and 27-28 dB, respectively. For the shear configuration, increases in the active control authority of up to 29 dB due to a properly tuned resonant circuit were observed. When subjected to uncertainties in the resistance and inductance values, with 10% relative dispersions, the control authority increase was found to be in the range of 6-29 dB.

Acknowledgements

This research was supported by FAPESP and CNPq, through research grants 04/10255-7 and 473105/2004-7, which the authors gratefully acknowledge. The authors also acknowledge the support of the MCT/CNPq/FAPEMIG National Institute of Science and Technology on Smart Structures in Engineering, grant no.574001/2008-5.

References

Andreaus, U. and Porfiri, M., 2007, "Effect of electrical uncertainties on resonant piezoelectric shunting," *Journal of Intelligent Material Systems and Structures*, Vol. 18, pp. 477-485.

Baillargeon, B.P. and Vel, S.S., 2005, "Active vibration suppression of sandwich beams using piezoelectric shear actuators: experiments and numerical simulations," *Journal of Intelligent Materials Systems and Structures*, Vol. 16, No. 6, pp. 517–530.

Benjeddou, A., 2007, "Shear-mode piezoceramic advanced materials and structures: a state of the art," *Mechanics of Advanced Materials and Structures*, Vol. 14, No. 4, pp. 263-275.

Benjeddou, A. and Ranger-Vieillard, J.-A., 2004, "Passive vibration damping using shunted shear-mode piezoceramics," In Topping, B.H.V. and Mota Soares, C.A., eds., Proceedings of the Seventh International Conference on Computational Structures Technology, Civil-Comp Press, Stirling, Scotland, p. 4.

Benjeddou, A., Trindade, M.A., and Ohayon, R., 1999, "New shear actuated smart structure beam finite element," *AIAA Journal*, Vol. 37, No. 3, pp. 378-383.

Cataldo, E., Soize, C., Sampaio, R. and Desceliers, C., 2009, "Probabilistics modeling of a nonlinear dynamical system used for producing voice," *Computational Mechanics*, Vol. 43, pp. 265-275

Forward, R., 1979, "Electronic damping of vibrations in optical structures," *Applied Optics*, Vol. 18, No. 5, pp. 690-697.

Hagood, N.W. and von Flotow, A., 1991, "Damping of structural vibrations with piezoelectric materials and passive electrical networks,"

Journal of Sound and Vibration, Vol. 146, No. 2, pp. 243-268.

Raja, S., Prathap, G., and Sinha, P.K., 2002, "Active vibration control of composite sandwich beams with piezoelectric extension-bending and shear actuators," *Smart Materials and Structures*, Vol. 11, No. 1, pp. 63-71.

Ritto, T., Soize, C., Sampaio, R., 2010, "Stochastic dynamics of a drill-string with uncertain weight-on-hook," *Journal of the Brazilian Society of Mechanical Sciences and Engineering*, Vol. 32, No. 3, pp. 250-258.

Soize, C., 2001, "Maximum entropy approach for modeling random uncertainties in transient elastodynamics," *Journal of the Acoustical Society of America*, Vol. 109, No. 5, pp. 1979-1996.

Sun, C.T. and Zhang, X.D., 1995, "Use of thickness-shear mode in adaptive sandwich structures," *Smart Materials and Structures*, Vol. 4, No. 3, pp. 202-206.

Thornburgh, R.P., and Chattopadhyay, A., 2003, "Modeling and optimization of passively damped adaptive composite structures," *Journal of Intelligent Materials Systems and Structures*, Vol. 14, No. 4-5, pp. 247-256.

Trindade, M.A. and Benjeddou, A., 2006, "On higher-order modelling of smart beams with embedded shear-mode piezoceramic actuators and sensors," *Mechanics of Advanced Materials and Structures*, Vol. 13, No. 5, pp. 357-369.

Trindade, M.A. and Benjeddou, A., 2009, "Effective electromechanical coupling coefficients of piezoelectric adaptive structures: critical evaluation and optimization," *Mechanics of Advanced Materials and Structures*, Vol. 16, No. 3, pp. 210-223.

Trindade, M.A., Benjeddou, A., and Ohayon, R., 1999, "Parametric analysis of the vibration control of sandwich beams through shear-based piezoelectric actuation," *Journal of Intelligent Materials Systems and Structures*, Vol. 10, No. 5, pp. 377-385.

Trindade, M.A., Benjeddou, A., and Ohayon, R., 2001, "Finite element modeling of hybrid active-passive vibration damping of multilayer piezoelectric sandwich beams – part 2: System analysis," I*nternational Journal for Numerical Methods in Engineering*, Vol. 51, No. 7, pp. 855-864.

Trindade, M.A. and Maio, C.E.B., 2008, "Multimodal passive vibration control of sandwich beams with shunted shear piezoelectric materials," *Smart Materials and Structures*, Vol. 17, art. no. 055015.

Tsai, M.S., and Wang, K.W., 1999, "On the structural damping characteristics of active piezoelectric actuators with passive shunt," *Journal of Sound and Vibration*, Vol. 221, No.1, pp. 1-22.

Viana, F.A.C. and Steffen Jr., V., 2006, "Multimodal vibration damping through piezoelectric patches and optimal resonant shunt circuits," *Journal of the Brazilian Society of Mechanical Sciences and Engineering*, Vol. 28, No. 3, pp. 293-310.